Surv Geophys (2010) 31:163–206
DOI 10.1007/s10712-009-9084-0

Laboratory Electrical Conductivity Measurement of Mantle Minerals

Takashi Yoshino

Received: 2 February 2009 / Accepted: 23 September 2009 / Published online: 7 November 2009

Abstract Electrical conductivity structures of the Earth's mantle estimated from the magnetotelluric and geomagnetic deep sounding methods generally show increase of conductivity from 10^{-4}–10^{-2} to 10^{0} S/m with increasing depth to the top of the lower mantle. Although conductivity does not vary significantly in the lower mantle, the possible existence of a highly conductive layer has been proposed at the base of the lower mantle from geophysical modeling. The electrical properties of mantle rocks are controlled by thermodynamic parameters such as pressure, temperature and chemistry of the main constituent minerals. Laboratory electrical conductivity measurements of mantle minerals have been conducted under high pressure and high temperature conditions using solid medium high-pressure apparatus. To distinguish several charge transport mechanisms in mantle minerals, it is necessary to measure the electrical conductivity in a wider temperature range. Although the correspondence of data has not been yet established between each laboratory, an outline tendency of electrical conductivity of the mantle minerals is almost the same. Most of mineral phases forming the Earth's mantle exhibit semiconductive behavior. Dominant conduction mechanism is small polaron conduction (electron hole hopping between ferrous and ferric iron), if these minerals contain iron. The phase transition olivine to high-pressure phases enhances the conductivity due to structural changes. As a result, electrical conductivity increases in order of olivine, wadsleyite and ringwoodite along the adiabat geotherm. The phase transition to post-spinel at the 660 km discontinuity further can enhance the conductivity. In the lower mantle, the conductivity once might decrease in the middle of the lower mantle due to the iron spin transition and then abruptly increase at the condition of the D″ layer. The impurities in the mantle minerals strongly control the formation, number and mobility of charge carriers. Hydrogen in nominally anhydrous minerals such as olivine and high-pressure polymorphs can enhance the conductivity by the proton conduction. However, proton conduction has lower activation enthalpy compared with small polaron conduction, a contribution of proton conduction becomes smaller at high temperatures, corresponding to the mantle condition. Rather high iron content in mantle minerals largely enhances the conductivity of the

T. Yoshino (✉)
Institute for Study of the Earth's Interior, Okayama University, Tottori 682-0193, Japan
e-mail: tyoshino@misasa.okayama-u.ac.jp

mantle. This review focuses on a compilation of fairly new advances in experimental laboratory work together with their explanation.

Keywords Electrical conductivity · High pressure · Mantle · Mineral · Review

1 Introduction

Electrical conductivity is one of useful methods to prove the Earth's deep interior. Exploration of the Earth's deep interior has been mainly carried out by seismological study to determine the fine structures in the Earth's mantle. Recent analytical development of electromagnetic studies to determine electric structure of the mantle has provided us an opportunity to understand different aspects of the Earth's mantle. Electrical conductivity of mantle rocks is controlled by the constituent phase (mineral) and its chemical composition under specific physical states such as pressure, temperature and oxygen fugacity. In addition, electrical conductivity is sensitive to minor conducting phase such as water, partial melt, graphite and metal. These features would yield additional constraints on mantle materials, if we have correct information on electrical properties of mantle materials. Laboratory conductivity measurements of conductivity, therefore, have the potential of providing valuable knowledge about chemical state, pressure, temperature and a presence of conductive phase such as fluid and partial melt.

Figure 1 shows the modal variation of the constituent minerals in the pyrolitic mantle. Stable phase changes with increasing pressure due to a phase transformation. Phase transformation changes the geometry of the atomic arrangement (crystal structure) as well as the nature of chemical bonding. Olivine (α phase) with a chemical composition of $(Mg,Fe)_2SiO_4$ is the most abundant mineral in the upper mantle and transforms to wadsleyite (modified spinel, β phase) and ringwoodite (spinel, γ phase) in the mantle transition zone at 410 and 520 km seismic discontinuities, respectively. High-pressure polymorphs of olivine decompose to post-spinel composed of perovskite and ferro-periclase at the 660 km seismic discontinuity. Pyroxene, with a chemical composition characterized by a stoichiometry of $(Mg,Fe)SiO_3$, is another important constituent mineral in the mantle. In the depth range from 300 to 500 km (depending upon the bulk composition), pyroxenes progressively dissolve into garnet with increasing pressure, forming majority (e.g., Takahashi and Ito 1987; Irifune and Ringwood 1993). Aluminous phase changes from plagioclase through spinel to garnet with increasing pressure. In the transition zone, majorite garnet is the second abundant constituent mineral. With increasing pressure, majorite garnet gradually dissolves into silicate perovskite. Near the core-mantle boundary, silicate perovskite transforms to silicate post-perovskite around 120 GPa (e.g., Murakmi et al. 2004). Although most mantle materials are silicates, non-silicate oxide ferro-periclase appears as a second abundant mineral in the lower mantle (Ito and Takahashi 1989). To determine mantle mineralogy from the electromagnetic studies, we need knowledge about the electrical conductivity of these minerals under high pressure. As a result, we can obtain additional constraints about the mantle mineralogy from the electromagnetic studies, independently of the seismological constraints.

Although minor conductive phase such as fluid (e.g., Glover et al. 1990), partial melt (Roberts and Tyburczy 1999; ten Glotenhuis et al. 2005), graphite film on the grain boundary (e.g., Glover and Vine 1992) and metal (Yoshino et al. 2003, 2004) is very important to explain the electrical conductivity values obtained from the geophysical observations, this paper mainly focuses on the electrical conductivity of the mantle

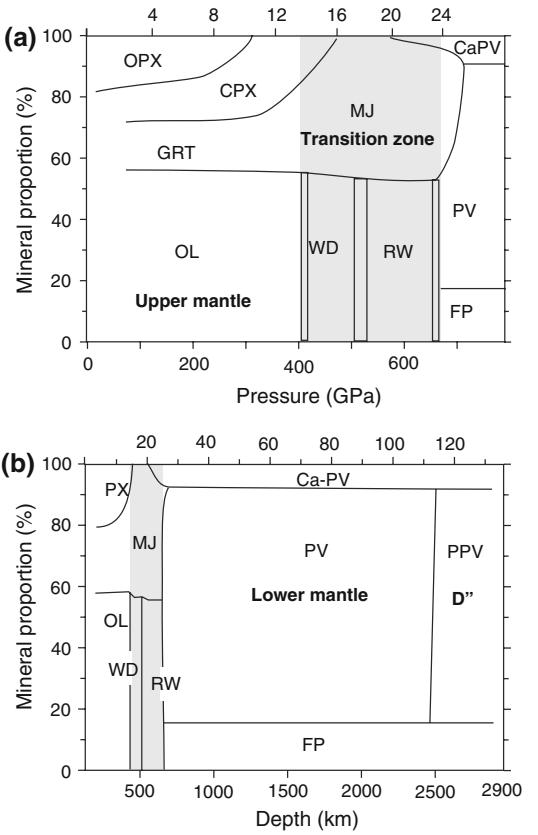

Fig. 1 Mineral proportions and phase transitions in Earth's mantle with pyrolitic composition up to 800 km (**a**) and up to the core-mantle boundary (~2,900 km depth). *Shaded areas* indicate the mantle transition zone between 410 and 660 km discontinuities. *PX* pyroxene, *OPX* orthopyroxene, *CPX* clinopyroxene, *GRT* garnet, *MJ* majorite garnet, *OL* olivine, *WD* wadsleyite, *RW* ringwoodite, *FP* ferro-periclase, *PV* silicate perovskite, *PPV* silicate post-perovskite, *Ca-PV* Ca-perovskite

minerals themselves to determine structure, mineralogy and anisotropy of the Earth's deep interior. At first, dominant electric conduction mechanisms in silicate minerals will be summarized. Second, methods of the conductivity measurement under high pressure will be described. Especially how to monitor proton conduction due to migration of hydrogen in nominally anhydrous minerals will be discussed in this section. Third, I review experimental results from the laboratory conductivity measurement for each main mantle mineral. Finally, this review paper introduces some topics of the Earth's mantle based on the recent publications concerning about electrical properties of mantle minerals.

2 Electric Conduction Mechanisms

Most silicate minerals act like an insulator at room temperature and their electrical conductivities are generally difficult to measure because of the conductivity values below the detection limit for the conventional multi-meter. Silicate minerals are regarded as ionic insulators with large energy gaps, for example, 6.4 eV for forsterite and 8 eV for quartz. However, when temperature increased to the mantle condition, these minerals behave as a semiconductor. Mobility of lattice defects and a small amount of impurity such as hydrogen, ferric iron and so on, enhances electrical conduction of silicate mantle minerals

at high temperatures. The conductivity of ionic-bonded crystals is proportional to number and mobility of charge carriers. It is known from the Nernst–Einstein equation that electrical conductivity (σ) depends on the number (N) of electric charge carriers per unit volume;

$$\sigma = Nze\mu, \tag{1}$$

where z is the charge number, e is the charge of electron and μ is mobility. The electrical conductivity is governed by Arrhenian behavior because mobility of charge carriers (diffusion) is a thermal activation process. The mobility of charge carriers (μ) can be described as the Arrhenian type equation

$$\mu = \frac{\mu_0}{T}\exp\left(-\frac{\Delta H}{kT}\right) \tag{2}$$

where μ_0 is the pre-exponential factor, ΔH is the activation energy, k is the Boltzmann constant, and T is the absolute temperature. In practice, the $1/T$ factor in the pre-exponential term is not always used, and expressions form of electrical conductivity

$$\sigma = \sigma_0 \exp\left(-\frac{\Delta H}{kT}\right) \tag{3}$$

where μ_0 is the pre-exponential factor. The activation enthalpy (ΔH) can be defined as a function of pressure (P) as follows:

$$\Delta H = \Delta E + P\Delta V \tag{4}$$

where ΔE is the activation energy and ΔV is the activation volume. Therefore, the electrical conductivity can be a function of temperature and pressure.

The electrical conductivity of the constituent mantle minerals is mostly influenced by proton (H^+) and small polaron conduction (electron holes hopping between ferrous and ferric iron) mechanisms, although ionic conduction occasionally appears as a dominant conduction mechanism at relatively higher temperatures close to the melting point. The electrical conductivity of a material is the sum of contributions from the different conduction mechanisms according to

$$\sigma = \sum_j N_j q_j \mu_j \tag{5}$$

where N_j is the density of the j-th type of charge carrier, q_j is the effective charge ($q = ze$), and μ_j is its mobility. The activation energies for each conduction mechanism depend on those of the charge mobility for each conduction mechanism. In addition, there is a temperature dependence of defect concentration for many extrinsic (and all intrinsic) charge carriers. Therefore, all conduction mechanisms can be distinguished by different slope (activation energy) defined in a specific temperature region on the Arrhenius plot.

2.1 Ionic Conduction

Ionic conduction can occur at high temperatures through the creation of cation vacancies. In the ferromagnesian mantle minerals (silicates and oxides), the charge carriers are generally vacancies in magnesium site $\left(V''_{\mathrm{Mg}}\right)$ as shown in Fig. 2. The ionic mobility varies with temperature as

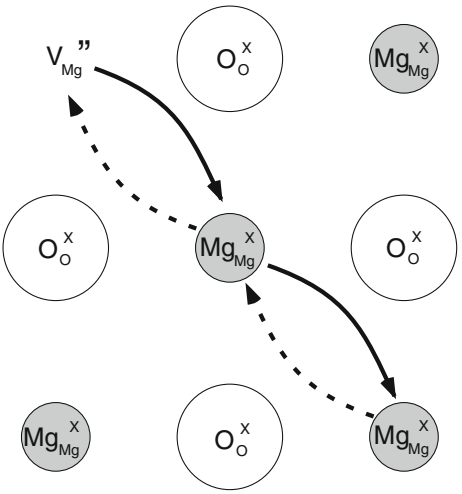

Fig. 2 A schematic diagram showing ionic conduction by migration of vacancies in magnesium site (V''_{Mg}). *Solid* and *dashed arrows* denote migration of V''_{Mg} and Mg ion, respectively

$$\mu = \frac{\mu_0}{T}\exp\left(-\frac{\Delta E_i}{kT}\right) \tag{6}$$

(Kittel 1996), where ΔE_i is the activation energy for the migration of vacancies. In this mechanism, Mg and Fe ions themselves move simultaneously. As a result, the energy barrier for the transportation of charge carriers is very high. The activation energy of ionic conduction is also high, usually higher than 2 eV. For this reason, extremely high temperatures are needed to observe the ionic conduction.

2.2 Hopping (Small Polaron) Conduction

Hopping conduction occurs through charge transfer between neighboring ions of different valence. In ferromagnesian mantle minerals, a ferrous ion (Fe^{2+}) generally substitutes an Mg ion in an Mg site. However, a certain proportion of ferric ion, which has an electron

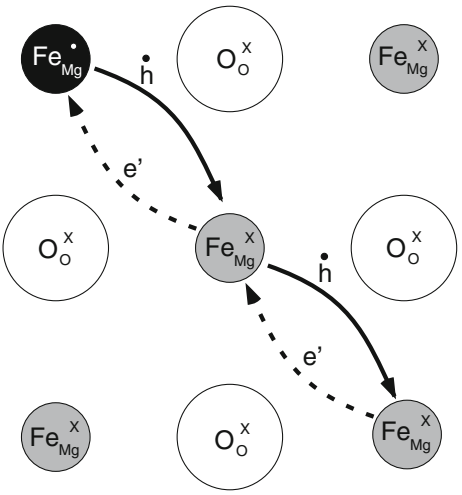

Fig. 3 A schematic diagram showing hopping (small polaron) conduction that transfer of an electron hole ($h^{\bullet}$) from $Fe^{\bullet}_{Mg}$ to Fe^{x}_{Mg} carries an electric charge. *Arrows* indicate migration of electron hole

hole exists dependent on oxygen fugacity, temperature, pressure, and crystal structure. Transfer of an electron hole $\left(\overset{\bullet}{h}\right)$ from $\left(\mathrm{Fe}^{\bullet}_{\mathrm{Mg}}\right)$ to $\mathrm{Fe}^{x}_{\mathrm{Mg}}$ carries an electric charge (Fig. 3), which is the hopping conduction.

$$\mathrm{Fe}^{x}_{\mathrm{Me}} + \overset{\bullet}{h} = \mathrm{Fe}^{\bullet}_{\mathrm{Me}} \tag{7}$$

If only electron holes migrate in crystal, the energy barriers for the migration would be low. However, the presence of an electric hole significantly affects the local structure of the ionic crystal. A presence of $\mathrm{Fe}^{\bullet}_{\mathrm{Mg}}$ generates an extra positive charge, which repulses cations and attracts anions (Fig. 4). This complex of the local strains is called "small polaron". The migration of electron holes associates that of the small polaron. The relatively large activation energy is needed to move a small polaron. The hopping conduction of usual ferromagnesian silicates has relatively large activation energy (>1 eV).

Hopping conduction in mantle minerals is proportional to the number of ferric ions. The density of charge carriers (n) is related to $\mathrm{Fe}^{3+}/\Sigma\mathrm{Fe}$ through

$$n = \frac{ZsX_{\mathrm{Fe}}}{V} \tag{8}$$

where s is the value of $\mathrm{Fe}^{3+}/\Sigma\mathrm{Fe}$, X_{Fe} is the atomic fraction of Fe per formula unit, V is the unit cell volume and Z is the number of formula units per unit cell. The charge carriers are tightly bound in the Fe d-bands, and the hopping process is thermally activated. The mobility of small polarons takes the form

$$\mu = \frac{A}{T}\exp\left(\frac{-\Delta E_{\mathrm{h}}}{kT}\right) \tag{9}$$

where A is a function of hopping distance and the attempt frequency, ΔE_{h} is the activation energy for hopping, k is the Boltzmann constant, and T is the absolute temperature (e.g., Goddat et al. 1999). Consequently, controlling factors for hopping conduction are oxygen fugacity and total iron content in mineral. $\mathrm{Fe}^{3+}/\Sigma\mathrm{Fe}$ in mantle minerals tends to increase with increasing oxygen fugacity. On the other hand, the density of charge carriers for hopping conduction increases with increasing the total iron content. We can identify

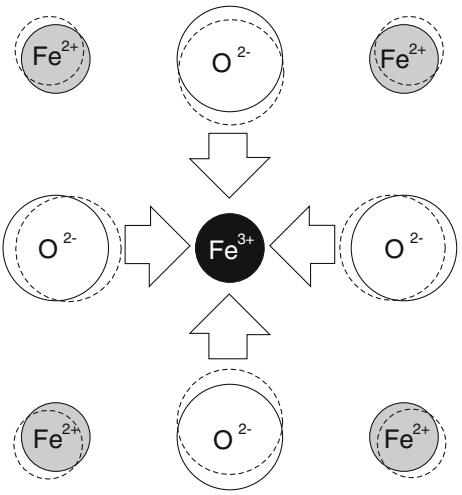

Fig. 4 A schematic diagram showing small polaron. Note that a presence of Fe^{3+} ion ($\mathrm{Fe}^{\bullet}_{\mathrm{Mg}}$) having an excess positive charge attracts the oxygen anion and repels the Fe^{2+} ion. *Solid* and *dashed circles* denote the position in each ion for situations without or with a presence of Fe^{3+} ion ($\mathrm{Fe}^{\bullet}_{\mathrm{Mg}}$), respectively

hopping conduction by conductivity measurements as a function of total iron content or oxygen fugacity.

The above discussion is available for ferromagnesian minerals that do not contain ferric ions for their basic composition. Carrier concentration is greatest close to $Fe^{3+}/\Sigma Fe = 0.5$, where is a *p–n* transition from holes to electrons. In the case of ferromagnesian minerals that contain both ferrous and ferric irons in their basic composition, electrical conduction occurs between the neighboring ferric and ferrous ion. For magnetite (Fe_3O_4), the following reaction occurs:

$$Fe^{x}_{Mg} + Fe^{X}_{Al} = Fe^{\bullet}_{Mg} + Fe'_{Al}, \tag{10}$$

in which the names of the sites follow those of $MgAl_2O_4$ spinel. Because the local electric charge is always zero, the local strains (small polaron) are very small. As a result, the activation energy is also very small ($\sim$0.01 eV). The magnitude of conduction is not expected to largely depend on oxygen fugacity.

Electron hopping between Fe^{2+} and Fe^{3+} (small polaron conduction) has been suggested to dominate electrical conductivity in mantle minerals based on the values for activation energy and volume, the dependence of conductivity on Fe^{3+} concentration obtained at low temperatures, and comparison of experimental data with small polaron theory. In ferromagnesian silicate minerals, the absolute conductivity values increase with increasing total Fe contents under the same oxygen buffer. Figure 5 shows an effect of the total iron content in iron-bearing silicate minerals on activation enthalpies for small polaron conduction. Activation enthalpy generally decreases with increasing total iron concentration; olivine along the forsterite–fayalite join (Omura et al. 1989), pyroxene along the ferrosilite–enstatite join (Seifert et al. 1981), garnet along the almandine–pyrope join at 10GPa (Romano et al. 2006), ringwoodite (Yoshino and Katsura 2009), and

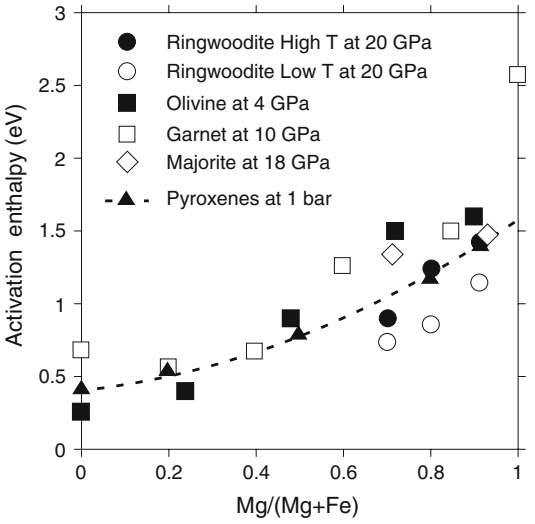

Fig. 5 Activation enthalpies for electrical conductivity in iron-bearing silicate minerals plotted as a function of Mg/(Mg + Fe). *Open* and *closed circles* represent activation energy for low and high temperature regimes of ringwoodite, respectively. *Open* and *closed squares* denote activation energies for olivine at 4GPa taken from Omura et al. (1989) and garnet at 10 GPa taken from Romano et al. (2006), respectively. *Dashed line* indicates activation energy for pyroxenes taken from Seifert et al. (1982)

post-spinel (Peyronneau and Poirier 1989). On the other hand, electrical conductivity measurements of olivine with Mg# ranging from 66.5 to 91.35 at atmospheric pressure showed no clear dependence of activation energy on iron content (Hirsch et al. 1993). However, the narrow temperature range in this study (1,423–1,573 K) might have prevented a reliable determination of activation energies.

A decrease in activation enthalpy with total Fe concentration is considered to be associated with a decrease in the average Fe^{3+}–Fe^{2+} distance. If the average Fe^{3+}–Fe^{2+} distance is isotropic, the activation enthalpy is expected to be proportional to the cube root of the total Fe content. Yoshino and Katsura (2009) proposed the following relationship approximating an equation for the *n*-type semiconductor (Debye and Conwell 1954),

$$\Delta H_h = \Delta H_{h0} - \alpha_h (X_{\mathrm{Fe}})^{1/3}, \tag{11}$$

where X_{Fe} is the mole fraction of iron in the Mg site, ΔH_{h} is the activation enthalpy at a certain value of X_{Fe}, ΔH_{h0} is the activation enthalpy observed at very low Fe concentrations, and α_{h} is a constant accounting for geometrical factors.

2.3 Large Polaron Conduction

A large polaron forms when the electron-lattice interaction due to the long-range Coulombic interactions between an electronic carrier and a solid's ions are of paramount importance. By contrast, a small polaron can form when a short-range electron-lattice interaction, such as the electron hopping, is dominant. Because lattice strain due to a presence of large polaron is larger than for a small polaron, the energy barriers for the large polaron migration are higher than those for the small polaron. As a result, activation energy for large polaron conduction is relatively higher than that for small polaron conduction.

Large polaron mechanism has been observed for pure periclase (Sempolinski et al. 1980) and proposed in ferro-periclase (Dobson et al. 1997; Dobson and Brodholt 2000). The iron–oxygen bond is strongly covalent in character, facilitating charge transfer. The mobility of holes in the O(2*p*) valence band is large, and their extrinsic formation would cause large polaron conduction where carriers are not bound to lattice sites. The mobility of large polaron charge carriers takes the form $\mu = \mu_0 T^{1/2}$. However, silicate minerals showing large polaron conduction mechanism have not been reported.

2.4 Proton Conduction

Proton conduction is a kind of ion conduction. Because the proton is overwhelmingly small ion but massive compared with electron, the proton is the only ion, which is expected to be highly mobile in solids. Nominally anhydrous minerals of the Earth's mantle (olivine and its high pressure polymorphs as well as pyroxenes and garnet) can store water as the hydroxyl group together with intrinsic point defects in their structure (e.g., Kohlstedt et al. 1996; Bolfan-Cassanova et al. 2000). Therefore, proton conduction could occur by small amounts of hydrogen in nominally anhydrous minerals (Karato 1990). The experimental data of hydrogen diffusion in single crystal olivine show strong anisotropy (Mackwell and Kohlstedt 1989). Conductivity anisotropy observed in the oceanic asthenosphere of the Eastern Pacific Rise was interpreted by proton conduction (Evans et al. 2005).

For proton conduction, charge transfer occurs by proton hopping amongst point defects. The pre-exponential factor for proton conduction increases with increasing water content. Dependence of the water content on electrical conductivity should follow the

Nernst–Einstein equation as shown in Eq. 5, because electrical conductivity depends on the number (N) of protons per unit volume. Yoshino et al. (2006, 2008a) reported that the activation enthalpy for proton conduction tends to decrease with increasing water content. If the average distance of the neighboring proton is isotropic, the activation enthalpy is expected to be proportional to the cubic root of the proton concentration except for the case that proton concentration is extremely low. This relationship can be approximated by an equation for n-type semiconductors (Debye and Conwell 1954),

$$\Delta H_{\mathrm{p}} = \Delta H_{0\mathrm{p}} - \alpha_{\mathrm{p}} \left(N_{\mathrm{p}}\right)^{1/3}, \tag{12}$$

where N_{p} is the number of protons, ΔH_{p} is the activation enthalpy at a certain value of N_{p}, ΔH_{p0} is the activation enthalpy observed at very low hydrogen concentrations and α_{p} is a constant accounting for geometrical factors. Taking into account the concentration dependence of the pre-exponential factor as defined by Eq. 5, the resultant electrical conductivities by proton conduction can be expressed as follows:

$$\sigma_{\mathrm{p}} = \sigma_{0\mathrm{p}} C_W \exp\left(-\frac{\Delta H^0 - \alpha_{\mathrm{p}} C_W^{1/3}}{kT}\right), \tag{13}$$

where $\sigma_{0\mathrm{P}}$ is a pre-exponential factor for proton conduction, C_{W} is the water content in weight, α is a geometrical factor, and H^0 is the activation enthalpy observed at very low water content.

The energy barrier for the transportation of charge carriers for proton conduction is relatively low because of its small bonding energy and small ionic radius. The activation energy of proton conduction is usually less than 1 eV. For this reason, the proton conduction is a dominant conduction mechanism at low temperatures.

3 Conductivity Measurements Under High Pressure

3.1 High Pressure Devices

The solid Earth was divided into the crust, the mantle and the core with increasing depth, based on remarkable changes in seismic velocities. The seismologists have tried to model the density and the pressure within the Earth as a function of depth (Bullen 1937). It was shown that the conditions of pressure up to 360 GPa and temperatures up to several thousands of degrees Kelvin extended into the Earth's interior. In order to decipher such Earth's structure models in terms of material science, high-pressure and high-temperature experiments on hypothetical Earth's forming materials have been carried out to reveal what structures and properties they possess under the corresponding conditions.

Some mantle minerals such as olivine, orthopyroxene and clinopyroxene are stable at room pressure. It is possible to measure the electrical conductivity in gas furnace under controlled oxygen partial pressure. However, high-pressure mantle phases generally decompose to a low-pressure phase at atmospheric pressure during heating. To measure electrical properties of mantle minerals under the corresponding conditions therefore requires high-pressure generation in laboratory. Although many kinds of pressure device have been developed, the solid pressure media is generally required to generate high pressure corresponding the mantle conditions. Three types of pressure device using the solid media are used widely in the Earth science community: piston-cylinder apparatus, Kawai-type multi-anvil press (KMA), and diamond anvil cell (DAC). Figure 6 summarizes

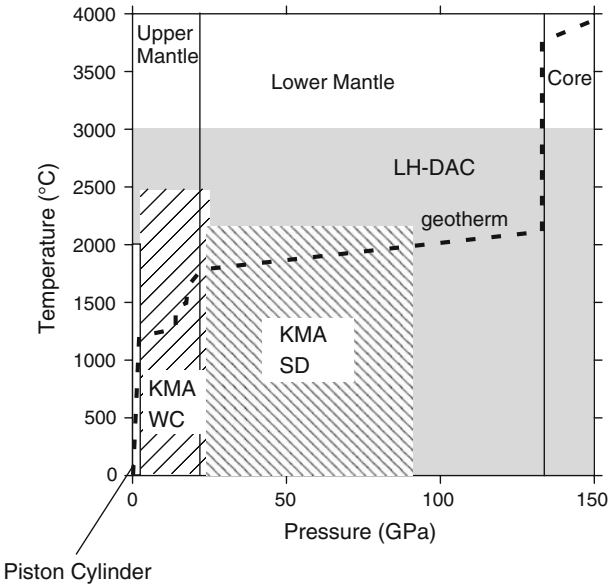

Fig. 6 The pressure–temperature ranges used for three pressure devices

Table 1 Summary of high-pressure press

Press type	*P*	*T*	Advantage	Disadvantage
Piston cylinder	<2 GPa (3/4″)	<2,500 K	Large volume (<400 mm^3)	Very narrow *P* range
	<4 GPa (1/2″)		Accurate *T* control	Difficult to take out many lead wires
Kawai-type multi-anvil press (KMA)	<30 GPa (WC)	< 3,000 K	Moderate volume (<50 mm^3)	Limited *P* range (up to the middle of the lower mantle)
	<100 GPa (SD)		Accurate *T* control	
			Hydrostatic	
			Easy to take out lead wires	
Diamond anvil cell (DAC)	<400 GPa	~4,000 K (laser heating)	Ultra high *P* generation	Very small volume
		~1,000 K	In situ synchrotron experiment	Inaccurate *T* control by laser heating
		(External heating)		Limited *T* generation by external heating

experimental pressure–temperature ranges for each pressure device. Advantages and disadvantages for each pressure device are summarized in Table 1.

In the piston-cylinder apparatus, a cylindrical sample assembly with various diameter (usually 1/2 and 3/4 inch size) is set in a bore hole of a thick-walled cylinder composed of hard materials such as tungsten carbide, and compressed by inserting a piston with the aid of a uniaxial press. The advantage of this press is characterized by relatively large sample space (<500 mm^3) and small thermal gradient. Pressure generation is limited up to ~2 and ~4 GPa for 3/4 and 1/2 inch size bore hole, respectively, because the attainable pressure

cannot reach the value of tensile strength of the bore materials. For conductivity measurement, the cylindrical shape is not suitable to take out many lead wires from the experimental cell.

The multi-anvil apparatus with 4 and greater anvils has been developed from the late 1950 to 1960s. A volume of the sample chamber is intrinsically larger than those of the opposed anvil apparatus such as DAC. The stress state in the samples is much closer to hydrostatic despite the usage of a solid pressure medium due to compression from multi-directions. The generated pressure is sustained by friction of the gasket. Because all the forces applied to the anvil are compression, the multi-anvil apparatus equipped with anvil composed of high-strength materials such as WC (tungsten carbide) can generate pressures largely higher than the piston-cylinder apparatus equipped also with WC piston. An octahedral anvil apparatus, called the Kawai-type apparatus, in which an octahedral pressure medium, was compressed by eight equivalent tungsten carbide anvils (Kawai 1966; Kawai and Endo 1970). The Kawai-type multi-anvil apparatus (KMA) is now widely used as a standard multi-anvil apparatus in the Earth science community.

The assembly of eight cubic anvils of WC with the octahedral pressure medium and gaskets is squeezed by the six-first-stage anvils made of hardened steel. Various high-strength materials, including hardened steel, tungsten carbide, boron carbide, sapphire, cubic zirconia, and sintered diamond are chosen as anvil materials dependent on the experimental purpose. Although tungsten carbide has been widely used as anvil material, high-pressure generation by the KMA is generally limited below 30 GPa by the strength of tungsten carbide. The generated pressure using the KMA has largely been extended by employing sintered diamond (SD) composed of diamond and Co metal for the material since the late 1980s (Ohtani et al. 1989; Kondo et al. 1989). The Knoop hardness of SD suggests that pressures up to 120 GPa can be generated by adopting SD (Sung and Sung 1996). Recently, the maximum pressure has been extended to higher than 90 GPa (Ito unpublished data). Near future, realization of large-volume experiment by the KMA covering the all mantle pressure conditions will be expected.

For the conductivity measurement under high pressure, the KMA has some remarkable advantages; (1) large sample volume, (2) accurate temperature control, and (3) flexibility to take out many lead wires. The large sample volume realizes a relatively simple sample dimension. As a result, we can easily estimate accurate conductivity value from the sample dimension. The large sample volumes in the KMA are also suitable for internal resistive heating. Millimeter-size sample capsules are placed in the middle of a heater in the high-pressure cell assembly. The resistive heater can provide uniform heating of the sample up to thousands of Kelvins. Usage of thermocouples allows accurate and fine temperature control. A shape of the octahedral pressure media allows taking many lead wires insulating each other out of the cell assembly. This flexibility is very important for the conductivity measurement. Disadvantage of the KMA is a limit of pressure generation. As far as we use tungsten carbide as anvil material, we cannot cover the depth range of the whole mantle. Recently an accessible pressure range for electrical conductivity measurement in the KMA has been extended to 35 GPa by adopting SD anvils (Katsura et al. 2007).

The DAC is one of the simplest high-pressure apparatus composed of the opposed anvils of single crystal diamond with flat faces at the top, which is developed from the Bridgman anvil. Two opposing anvils compress a gasket, which contains the sample chamber at the center. The DAC can cover widely the mantle pressure conditions up to the core-mantle boundary (above 135 GPa). In addition, the DAC equipped with laser heating system (LH-DAC) can realize extremely high temperature conditions (<4,000 K). Therefore, an important benefit of the DAC is its ability to generate extreme physical

conditions. In addition, the DAC is excellent for in situ optical observation and the X-ray diffraction of the sample under the high-temperature and high-pressure conditions, because diamond is highly transparent for electromagnetic waves of a broad range of frequency.

One disadvantage of the DAC for the conductivity measurement is derived from heating of the sample. Two heating systems have mainly applied in the DAC. An external furnace was used to heat the cell, and temperature was monitored by thermocouple in contact with one of the diamonds (Peyronneau and Poirier 1989). Although this method allows accurate temperature measurement, the external resistive heating is unsuitable for high temperature generation. The maximum accessible temperature is generally around 1,100 K (Fei and Mao 1994). As a result, extrapolation of the low temperature data to the mantle condition is required. The LH-DAC has been developed for determination of the physical properties of high-pressure materials under high-temperature condition (Ming and Bassett 1974). The temperature is measured from the black-body radiation. Due to the steep temperature gradient, different laboratories have reported contradictory results in the past. However, the development of the double-sided laser heating technique is now improving the above problems (e.g., Mao et al. 1998). At present, the LH-DAC is the only choice to realize the mantle temperatures under ultrahigh pressure. Recently Ohta et al. (2008) measured the electrical conductivity of perovskite and post-perovskite in wide range of pressure up to 143 GPa and temperature up to 3,000 K using the LH-DAC. At this moment, it is still difficult to determine accurate activation energy for electric conduction because of large errors of temperature measurement, huge temperature gradient and difficulty of stable temperature control.

The other problem of the DAC is that the sample size is very limited. In general, electrical conductivity of the sample has been calculated from the cross-sectional area of electrode and sample thickness. To generate pressure above 100 GPa, the sample size is occasionally less than 50 μm. The smaller size of sample would lead to the larger error of the calculated conductivity. If edges of two electrodes of thin metal foil were connected to the sample, it is very difficult to define the effective cross-sectional area of electrodes.

3.2 Principle of Conductivity Measurement

The *R* (resistance)–*C* (capacitance) parallel circuit has been generally used to determine the electrical conductivity of mantle minerals as shown in Fig. 7a. In the complex impedance plane, the magnitude and direction of a planar vector can be defined by an impedance $Z(\omega) = Z' + jZ''$, where $Z(\omega)$ is impedance as a function of frequency for alternating current, Z' and Z'' are real and imaginary parts of impedance, respectively. The phase angle (θ) in complex impedance plane can be obtained from $\theta = \tan^{-1}(Z''/Z')$. When the phase angle is 0°, the sample resistance for the *R*–*C* parallel circuit equals to the real part of impedance.

Roberts and Tyburczy (1991) observed three impedance arcs in the complex impedance plane from the frequency dependent electrical measurements (10^{-4}–10^{4} Hz) of polycrystalline olivine compacts at atmospheric pressure, and interpreted them as grain interior (first arc), grain boundary (second arc) and electrode reaction mechanism (third arc) from high to low frequency, respectively (Fig. 7b). Later, absence of the second arc was confirmed by the measurement of single crystal olivine (Roberts and Tyburczy 1993). However, at high pressures, a remarkable presence of the second and third arcs in low frequency range has not been observed for the dry polycrystalline mantle minerals (e.g., Romano et al. 2006; Yoshino et al. 2008a). Because pores, cracks or grain boundaries in a sample are tightly closed, even if the grain boundary has high impurity level (Hiraga et al. 2004),

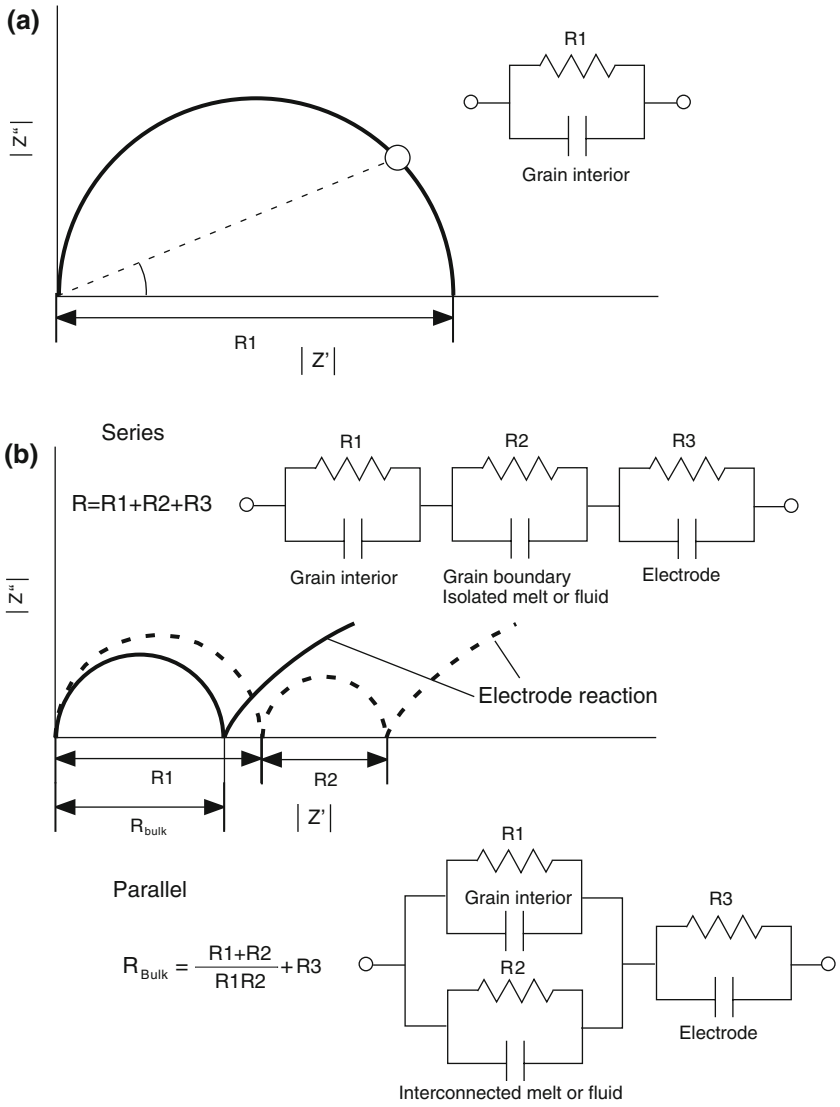

Fig. 7 Schematic diagram showing equivalent circuit and impedance spectra. **a** Impedance spectra for a case that only the grain interior mechanism is dominant. *Open circle* indicates real and imaginary parts of impedance at a certain frequency. The phase angle ($\theta = \tan^{-1}(Z''/Z')$) is defined in complex impedance plane. **b** Schematic responses of combination of the three mechanisms: grain interior, grain boundary or melt/fluid phase and electrode process. The *dashed line* indicates a case that series conduction is dominant, and the solid line indicates a case that parallel conduction is dominant (Roberts and Tyburczy 1999)

the grain boundary conduction due to the extremely narrow width of the grain boundary would not contribute the impedance spectroscopy. Electrical measurements are usually made with cells having two electrodes applied to the faces of sample. If electrodes seriously reacted with a sample, the additional part may appear at lower frequency side.

The conductivity values of silicate minerals, in particular iron-poor and dry minerals, are extremely low at low temperatures. In this situation, the low frequency measurement is

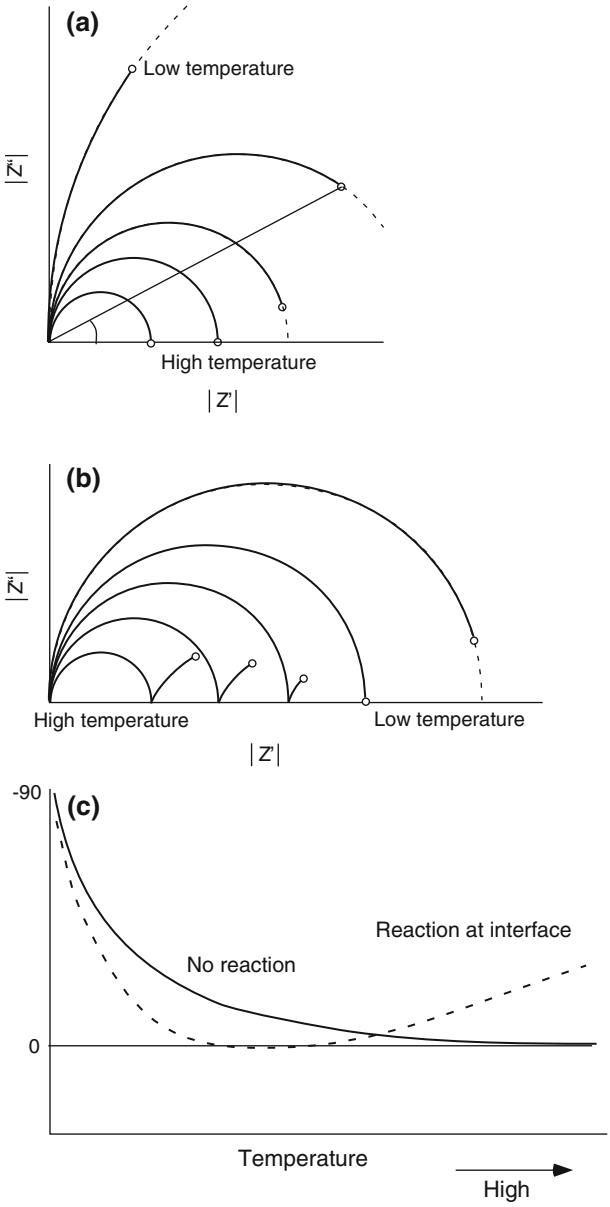

Fig. 8 Schematic impedance spectra of silicate minerals as a function of temperature under high pressure. *Open circles* indicate data at a single low frequency. **a** Sample reacting with electrode at the interface. Note that low frequency data is always located on the first impedance arc. **b** Sample showing reaction at the interface between electrode and sample. Note that the position of low frequency data changes from the first impedance arc to the tail (second arc) with increasing temperature. **c** Phase angle versus temperature for hypothetical dry and wet materials

also very useful to determine the conductivity values. For this purpose, the low frequency measurement has been developed to measure high resistive materials (Katsura et al. 1998). When we measure high resistive materials, it is difficult to obtain the complete impedance arc with semicircular shape because of the limit of the measurement system. At constant frequency the Z' approaches to the sample resistance (R) with increasing conductivity values (in other words, increasing temperature). In this situation, the phase angle of a sample impedance decreases to zero with increasing conductivity values (Fig. 8). In principle, until the phase angle decreases to zero, the measurement results should be located on the first arc.

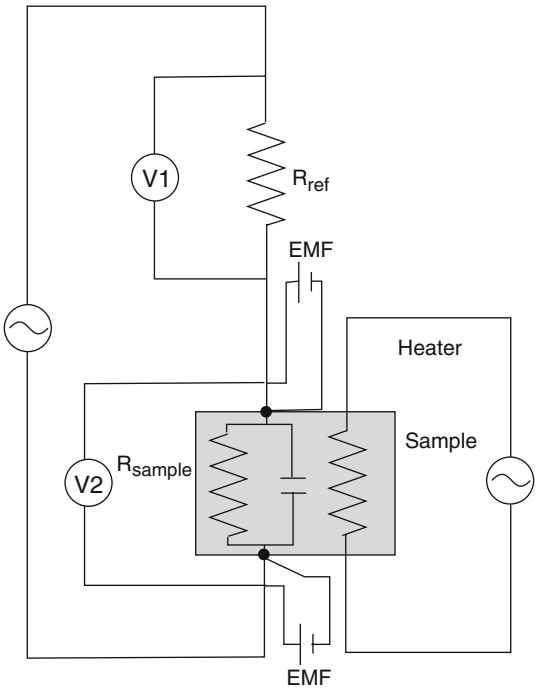

Fig. 9 Circuit for electrical conductivity measurement at low frequency. *Shaded area* indicates the cell assembly

Figure 9 shows the electric circuit for the conductivity measurement at low frequencies. The sample is connected to a reference resistance, variable in a range 50–10^6 ohm, in series. A sinusoidal alternating voltage is applied to the electric circuit by a function generator. The voltage applied to the sample is measured using both sides of the thermocouple or lead wire. The sample impedance (Z_s) is obtained from the reference resistance (R_R) and the ratio of the voltages of the sample and reference,

$$Z_s = R_R \frac{V_S}{V_R}. \tag{14}$$

Assuming that the impedance of the sample is composed of the R–C parallel circuit, the resistance of the sample is obtained from the following equation:

$$\frac{1}{Z_s} = \frac{1}{R_S} + i\omega C. \tag{14}$$

This method can yield data with a good signal–noise ratio for the high resistive materials. In order to obtain the accurate sample conductivity, we need to confirm that the data is located on the first arc. Only data showing the phase angle (θ) of nearly 0° should be used for determination of the sample resistance, because the arc is sometimes distorted by the presence of distributed elements in the material-electrode system (e.g., CPE: constant phase element) and other relaxations (reaction or polarization at the electrode).

3.3 High-Pressure Experimental Cell

Electrical conductivity measurement at high pressure and temperature has been performed using both the KMA and the DAC. Figure 10 shows cross sections of the two typical cell

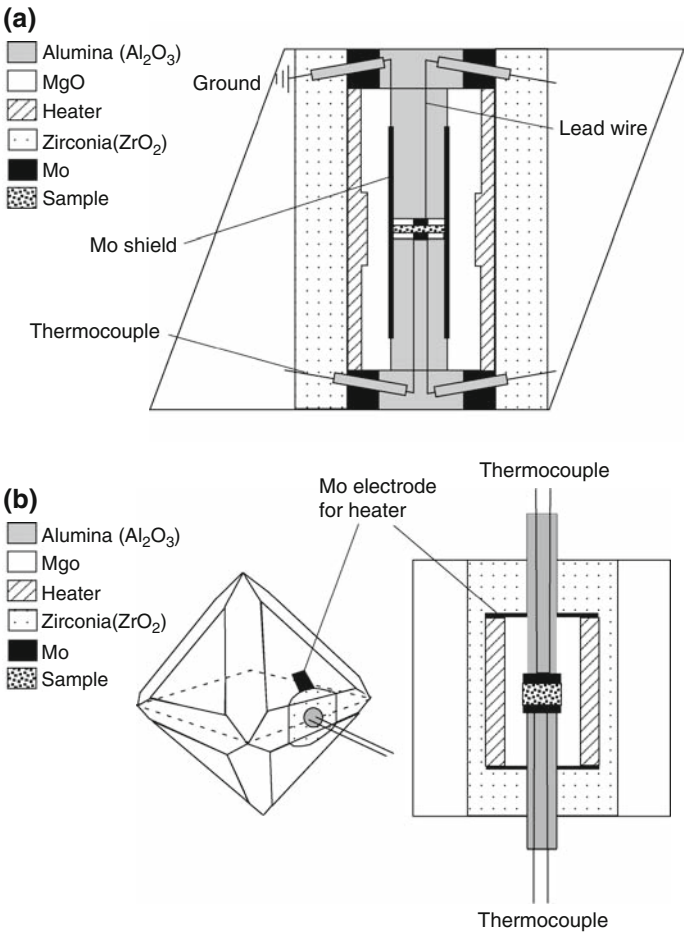

Fig. 10 Typical cell assemblies for conductivity measurement in the KMA. **a** Bayreuth cell. **b** Misasa cell

assemblies for measuring electrical conductivity in the KMA. The pressure medium is composed of primary MgO. A cylindrical heater composed of graphite, metal or $LaCrO_3$ is put in a thermal insulator sleeve. The sample is located on the center of the cell assembly, and sandwiched by two metal disks (Fe, Ni, Mo, Re, Ir, Pt, Au, etc.). The sample is embedded in a sample container made of ceramic insulator (MgO, Al_2O_3). Metal disk contacting with a sample is an important item to establish bound on oxygen fugacity of the sample. Mo is widely used to control near Mo–MoO_2 oxygen buffer, which is similar to iron-wüstite (IW) buffer. The thermocouple mechanically connected to one metal disk to measure the sample temperature and also to serve as electrodes for electrical conductivity measurement. The other metal disk is connected to a metallic lead for an electrode of electrical conductivity measurement. The thermocouple and the lead wires are insulated from the heater by ceramic insulators. After decompression, the thickness and diameter of the sample are measured on a cross section of the recovered cell assembly. The electrical conductivity of the sample (σ_s) is calculated from the sample resistance and the sample dimensions by the equation,

$$\sigma_s = \frac{l}{SR_s}, \tag{16}$$

where S and l are the cross-sectional area of the electrode and the thickness of the sample, respectively. Xu et al. (1998a) also developed a similar assembly to measure electrical conductivity by means of impedance spectroscopy. They set a cylindrical metal shield connected to the ground, which is set inside the heater and envelops the sample. The advantages of the shield are avoiding electric disturbance from the heater, minimizing the temperature gradient, and reducing leakage current through the pressure medium and lead wires. As described later, the disadvantage of the shield is low insulation resistance due to the retention of the water escape from the sample at low temperatures.

Figure 11 shows a cell assembly for measuring electrical conductivity in the LH-DAC (Ohta et al. 2008). For the ultrahigh pressure (>50 GPa) measurement, the $\sim$50 μm size sample is loaded into a hole at center of the rhenium gasket. Metal electrodes made of thin foil are placed on the Al_2O_3 layer, which electrically insulated the sample and electrodes against rhenium. No pressure medium is loaded in order to ensure a good contact between sample and electrodes. The electrical conductivity has been usually measured using two-probe configuration by an electrometer in the direct current (DC).

3.4 Conductivity Measurement

In situ conductivity measurements are conducted from room temperature (300 K) to high temperature with a few heating and cooling cycles. During each cycle, the temperature is changed in a certain interval (50–100 K), and electrical conductivity is measured at each temperature. We should pay attention to the following points for the conductivity measurement under high-pressure condition.

3.4.1 Insulation Resistance Test

At low temperatures, it is difficult to determine the resistance of silicate minerals due to the measurement limit of the multi-meter ($\sim$10 Gohm, corresponding to $\sim 10^{-7}$ S/m for a sample conductivity). However, conductivity of the sample placed in a cell is not always higher than that of the background. To distinguish among different potential conduction paths in the sample environment, the resistance in a sample environment is needed to define a background insulation resistance. In this test, the high insulation ceramics such as MgO and Al_2O_3 are placed in the sample position (e.g., Yoshino et al. 2004, 2008; Manthilake et al. 2009). The background insulation resistance test is used to establish a conductivity baseline, and it can be considered that conductivity measured below the values of this test is not derived from the sample.

3.4.2 Iron Loss to Electrode

Omura (1991) reported lower electrical conductivity of the wadsleyite compared with the values of Xu et al. (1998a, b). Omura (1991) directly connected a thermocouple (WRe_3–WRe_{25}) to the sample, and synthesized wadsleyite from the olivine during conductivity measurement. Xu et al. (1998a) performed a similar experiment and demonstrated the severe iron loss to the electrode as a reason of the low conductivity values. Consequently, Xu et al. (1998a, b) pointed out that use of the pre-synthesized sample for conductivity measurement is useful to avoid the iron loss to the electrode. On contrary, in the case of

Fig. 11 Schematic designs of high-pressure devices. **a** Piston-cylinder apparatus. The device consists of a double ram with an axially supported tungsten carbide vessel. **b** Kawai-type multi-anvil apparatus (KMA). The DIA-type guide block compressing the eight cubes. Each of eight separate tungsten carbide cubes has a truncated corner that rests against the face of an MgO octahedral pressure medium. The truncated cubes are separated from one another by compressible pyrophyllite gaskets. Sample material is placed inside a furnace assembly in the center of the octahedron. **c** Double-sided laser heating in the diamond anvil cell (DAC) ▶

Mo electrode, a remarkable difference between the pre-synthesized and the in situ synthesized samples has not been observed (e.g., Yoshino et al. 2008a, b; Manthilake et al. 2009). Nevertheless, it is necessary to avoid maintaining the high temperature for a long time to minimize iron loss to electrode.

3.4.3 Confirmation of Reproducibility

Electrical conductivity measurements are performed along the heating–cooling cycle to determine activation enthalpy of electric conduction in the sample. Generally, initial conductivities of the sample are high for first heating, because the cell assembly initially contains tiny amount of water. When the high resistive sample is heated to a given high temperature (>1,000 K), the conductivity drops due to the dehydration of the cell assembly including the sample. For the subsequent cooling, the conductivity–temperature path is different from that for the first heating. Therefore, the Arrhenian relation obtained for the first heating is usually unreliable. After the dehydration of the sample and the surrounding material, the subsequent heating–cooling paths track the path for first cooling without a drastic change of the sample environment. Hence, confirmation of data reproducibility ensures a quality of data to determine accurately activation enthalpy.

3.4.4 Identification of Conduction Mechanisms

Figure 12 shows a schematic drawing of Arrhenian conductive behavior of silicate minerals including some conduction mechanisms. Each conduction mechanism would be dominant at a specific temperature range. Although conductivity measurements have been performed in a restricted temperature range to determine the activation enthalpy of the electric conduction, in order to identify each conduction mechanism, the conductivity measurement should be carried out in a wider temperature range. Because proton conduction with low activation energy appears at low temperatures (Yoshino et al. 2006, 2008a), high insulation resistance in sample environment is required for the conductivity measurement to recognize proton conduction mechanisms.

3.5 Conductivity Measurement of Proton Conduction in Nominally Anhydrous Mantle Minerals

The conductivity measurement of hydrogen-bearing nominally anhydrous mineral is a very difficult issue, because hydrogen in silicate minerals easily escapes from the inside under high temperature condition above 1,000 K due to the high diffusion rate of hydrogen (Mackwell and Kohlstedt 1990). Therefore, there has been no report concerning about this issue until 2005. Electrical conductivity of hydrous wadsleyite and ringwoodite has been firstly reported based on the impedance spectroscopic measurement in quite short time at a single temperature condition for each run in order to minimize water loss (Huang et al. 2005). Subsequently, the same group hereafter referred as Yale group reported electrical

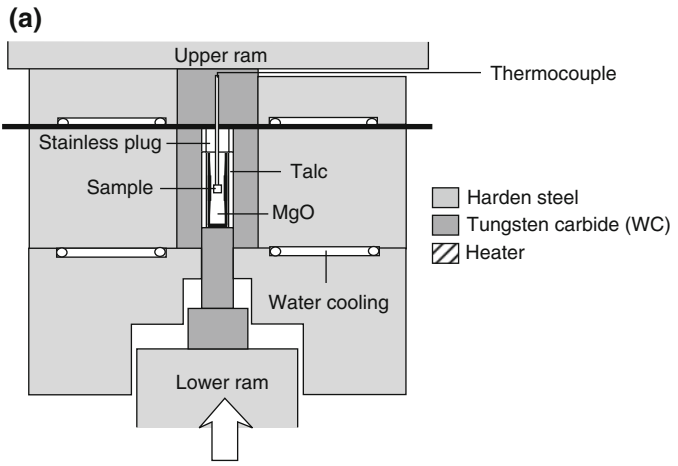

Piston cylinder

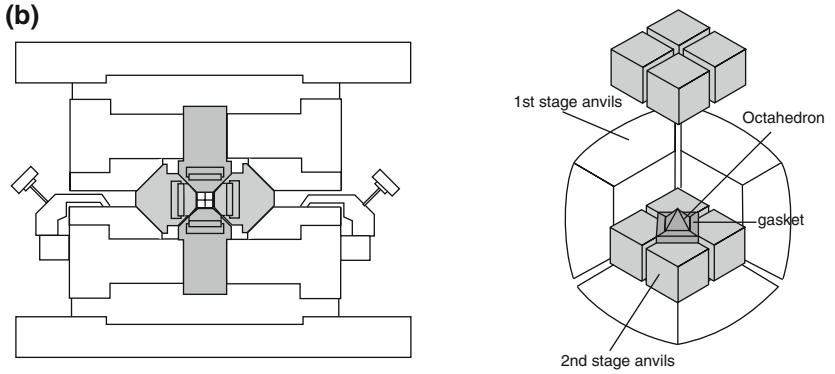

Kawai-type (6-8) multianvil (KMA) press

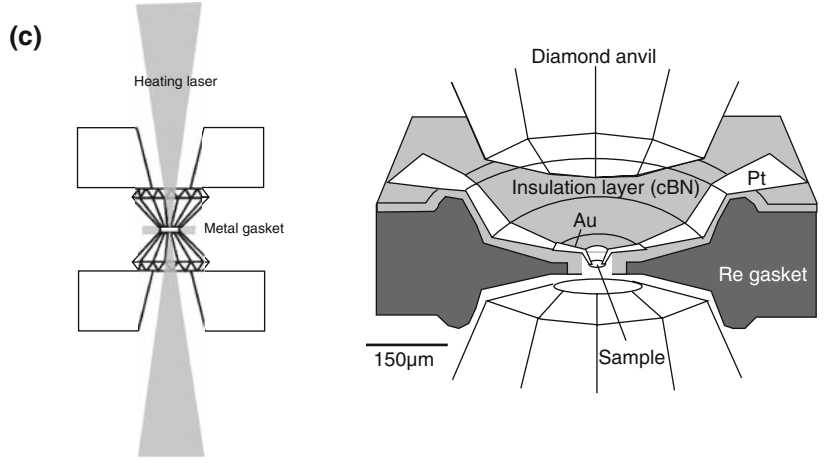

Diamond anvil cell (DAC)

conductivity of hydrous olivine aggregate in a slightly wider temperature range (Wang et al. 2006). On the other hand, the other group hereafter referred as Misasa group measured the electrical conductivity of hydrous olivine, wadsleyite and ringwoodite at lower temperature range (<1,000 K) by low frequency measurement (0.1 Hz) and impedance spectroscopy (Yoshino et al. 2006, 2008a; Manthilake et al. 2009). Both groups reported that the hydrous minerals have higher conductivity than the anhydrous samples. However, the conductivity values and activation enthalpies for proton conduction determined by Yale group were significantly higher than those obtained by Misasa group. In this section, some notes of the measurement of the proton conduction are discussed while considering the cause of the difference of the result between two laboratories.

The most difficult problem to measure proton conduction is to avoid water escape from the crystal, because diffusion rate of hydrogen in nominally anhydrous minerals is quite fast at high temperatures. There are two approaches to overcoming the above problem: one is to measure conductivity in a closed system for H_2O, and the other is to measure conductivity at low temperatures at which the hydrogen diffusion rate is sufficiently low. The former is impractical, because of the difficulty of sealing-in H_2O by using an insulating material. The latter is more feasible method but the measurement temperature range is limited to the low temperature. Yoshino et al. (2006) showed that the hydrogen-doped minerals release free-water at some temperature above 900 K (occasionally 800 K) and demonstrated that high conductivity of interconnected free-water masks conductivity of the grain interior (proton conduction) even though the amount of free-water is very small.

3.5.1 High Insulation Resistance

Electrical conductivity measurements under low temperature conditions (<1,000 K) require high insulation resistance to detect the sample resistance. The minimum range of conductivity measurement is generally around 10^{-4} S/m, as shown in Fig. 12. In contrast, a single crystal MgO capsule allows us to measure conductivity down to 10^{-7} S/m. The measurement range is clearly insufficient to measure conductivity of hydrous olivine, wadsleyite and ringwoodite with small water content. The excellent insulation resistance is needed to measure sample conductivity in a wider measurement range. In addition, purge of adhesive water at low temperatures is also required. Misasa group performed pre-annealing at 500 K for several hours to remove free-water in the sample environment before the conductivity measurement. It has been confirmed that, at 500 K, dehydration of crystal itself hardly occurs because of low hydrogen diffusion at this temperature. Use of the Mo guard ring by Yale group does not provide good insulation resistance, and would prevent water purge.

3.5.2 Determination of Water Content Before and After Conductivity Measurement

To confirm that the dehydration does not occur during conductivity measurement is very important procedure. The Fourier Transform Infrared (FTIR) analysis is usually used to determine water content in the sample. The measurement at relatively high temperatures (>1,000 K) is likely to accompany with dehydration of the sample itself. Actually, Huang et al. (2005) and Wang et al. (2006) reported loss of water (at most 30%) after the conductivity measurements. In contrast, Misasa group confirmed no change of water content after the conductivity measurement at low temperatures (<800 K) (Yoshino et al. 2008a; Manthilake et al. 2009).

3.5.3 *Impedance Spectroscopy vs. Low Frequency Measurement*

Karato and Dai (2009) claimed that Misasa group's data mostly based on the low frequency measurement is invalid as the sample conductivity values, because their impedance spectroscopy for wet wadsleyite measured at high temperatures showed the additional tail at low frequencies, and suggested that the actual conductivity of the sample should be higher than the reported values by Misasa group. The additional tail at low frequency is caused by the reaction between the sample and electrode. However, it has been demonstrated that, at low temperatures, the conductivity values of hydrous ringwoodite determined from the low-frequency measurement is excellently consistent with those determined from impedance spectroscopy (Yoshino et al. 2008a). It is shown that the clear second arc does not appear, and the shape of arc is close to semicircular shape (Fig. 13a). If the equivalent circuit is a simple R–C parallel circuit composed of a single relaxation process, the impedance arc shows the semicircular shape. In contrast, the impedance arc obtained at higher temperatures is clearly distorted from the semicircular shape (Fig. 13b). It suggests that the electric circuit contains several relaxation processes. As shown in Fig. 7, a presence of interconnected conductive phase such as fluid, melt and metal produces a parallel circuit composed of grain interior and interconnected phase conductions. Impedance spectroscopic studies of partial molten rocks have shown that the grain interior resistance is also masked by interconnection of the melt phase (e.g., Roberts and Tyburczy 2000; ten Grotenhuis et al. 2005). In addition, the phase angle in the complex impedance plane calculated from the low frequency measurement is nearly zero degree and decreases with increasing temperature. This behavior indicates that the data is located on the first arc, because the first arc shrinks with increasing temperature. Therefore, it is concluded that differences of conductivity values and activation energy are not caused by that of measurement method between the impedance spectroscopy analysis and low frequency measurement. Consequently, the presence of the free-water would be the reason why Yale group overestimated proton conduction of nominally anhydrous minerals.

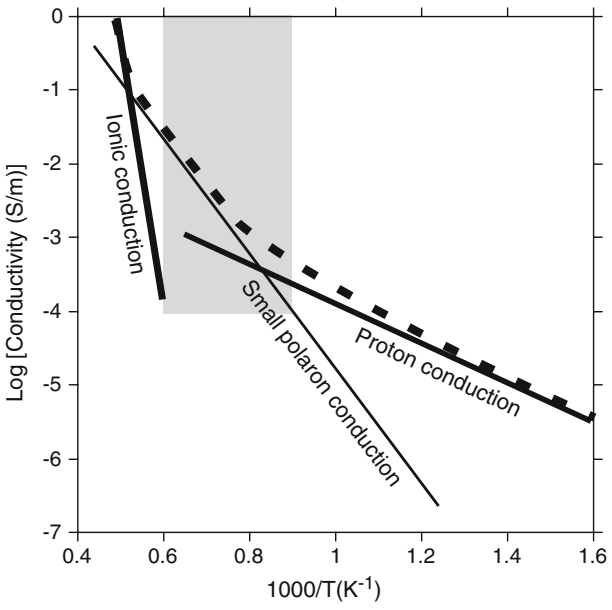

Fig. 12 A schematic drawing of Arrhenius plot for a hydrogen-iron bearing mantle silicate mineral. *Hatched area* indicates the measurement region by Xu et al. (1998a, b)

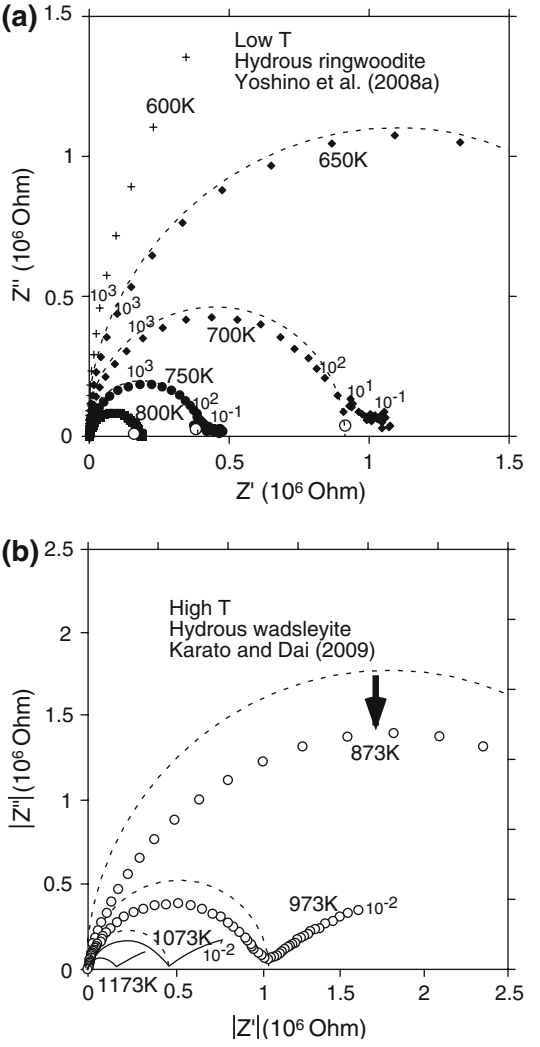

Fig. 13 Complex impedance spectra showing the semicircular pattern of the real vs. imaginary components of complex impedance at frequencies ranging from 1 MHz to 0.1 or 0.01 Hz at the temperatures indicated (Karato and Dai 2009; Yoshino et al. 2008a). *Dashed lines* indicate impedance spectra assuming the R–C parallel circuit as an equivalent circuit. **a** Impedance spectra of hydrogen-doped ringwoodite sample measured at temperatures ranging from 500 to 800 K. *Open circles* indicate the measurement results separately obtained from the low frequency measurement system. **b** Impedance spectra of hydrogen-doped wadsleyite sample measured at 20 GPa and temperatures ranging from 873 to 1,173 K. Note that the data are largely deviated from the simple R–C parallel circuit

4 Electrical Conductivity of Mantle Minerals

In the Earth's mantle, some seismic velocity discontinuities have been globally observed, and are thought to be caused by the phase transformations of mantle minerals (Fig. 1). Numerous high-pressure experiments have clarified that the upper mantle mineral phases transform to the high-pressure polymorphs. The important phase transitions occur at the 410 (olivine to wadsleyite), 520 (wadsleyite to ringwoodite), 660 km (ringwoodite to perovskite and ferro-periclase) and D" (perovskite to post-perovskite) discontinuities. A phase transformation affects the electrical properties due to a change of the atomic arrangement (crystal structure) as well as the nature of chemical bonding. In this chapter, the electrical conductivities of the major mantle constituent minerals are briefly reviewed. High-pressure electrical conductivity data for dominant constituent mantle minerals are summarized in Tables 2, 3, 4, 5.

Table 2 High-pressure electrical conductivities of olivine given in the Eq. 3

Sample	Mechanism	P (GPa)	T (K)	$\log\sigma_0$ (S/m)	ΔE(eV)	ΔV (cm^3/mol)	Reference
Single crystal							
[100]	SP	4	1,273–1,673	3.33(28)	1.79(8)		Xu et al. (2000a)
[001]	SP	4–10	1,273–1,673	2.67(14)	1.50(4)	0.86(15)	
[010]	SP	4–10	1,273–1,673	1.67(12)	1.17(4)	0.62(13)	
[010]	SP	4–10	1,273–1,673	2.39(6)	1.35(2)	0.96(6)	
[100]	SP	3	973–1,473	1.18	1.35		Yoshino et al. (2006)
	P	3	723–973	0.37	0.73		0.02 wt.% H_2O
[010]	SP	3	973–1,473	2.23	1.42		
	P	3	673–873	0.87	0.93		0.02 wt.% H_2O
[001]	SP	3	973–1,473	2.45	1.47		
	P	3	473–773	0.88	0.87		0.01 wt.% H_2O
Polycrystal							
	SP	4–10	1,273–1,673	2.29(19)	1.66(9)	0.09(32)	Xu et al. (2000a)
	SP	4–10	1,273–1,673	2.69(12)	1.62(4)	0.68(14)	
	P	10	800–1,400	0.83(7)	1.11(0)		Yoshino et al.
	SP	10	1,400–1,750	3.34(8)	1.77(2)		(2009)
	I	10	1,750–2,000	4.73(19)	2.25(7)		
	P	4	873–1,273	*****	0.90(5)		Wang et al. (2006)

SP small polaron conduction, *P* proton conduction, *I* ionic conduction

***** Electrical conductivity is expressed by the following equation $\sigma = \sigma_0 C_w^r \exp\left(-\frac{\Delta H}{kT}\right)$ (17),
where σ_0 is pre-exponential factor ($\log\sigma_0 = 3.0 \pm 0.4$), C_w is water content in weight %, and r is constant (0.62 ± 15)

4.1 Olivine

Olivine is the most abundant mineral in the upper mantle. The electrical conductivity of olivine has been extensively studied under the various conditions at atmospheric pressure. Although the present paper focuses on experimental results from high-pressure studies, important insights from these studies are firstly summarized. Electrical conductivity in the three principal crystallographic directions of a San Carlos olivine shows anisotropic signature of a factor of 2–3; the highest [001] and the lowest [010] (Schock et al. 1989; Shankland and Duba 1990; Du Frane et al. 2005). The electrical conductivity increases with increasing oxygen fugacity (Wanamaker and Duba 1993; Hirsch and Shankland 1993; Du Frane et al. 2005) and total iron content (Hirsch et al. 1993). Conduction mechanisms in olivine have been considered as a mixture of electron hopping (small polaron conduction) and magnesium vacancies (ion conduction) at high temperatures greater than 1,473 K. Based on these studies, electrical conductivity of dry olivine has been modeled as a function of temperature and oxygen fugacity (Shankland and Duba 1990; Constable et al. 1992; Constable 2006).

Table 3 High-pressure electrical conductivities of wadsleyite and ringwoodite given in the Eq. 3 for Xu et al. (1998a) and Yoshino and Katsura (2009), the Eq. 17 for Huang et al. (2005), the Eq. 14 for Yoshino et al. (2008a)

Phase	Mechanism	P (GPa)	T (K)	$\log\sigma_0$ (S/m)	ΔH(eV)	alpha	r	Reference
Wadsleyite								
Mg#90	SP?	15	1,323–1,473	3.29(20)	1.29(6)			Xu et al. (1998a)
Mg#90	P			2.57	0.91 (3)		0.66(5)	Huang et al. (2005)
Mg#91	SP	16	500–1,700	0.89	0.68	0.02(2)		Yoshino et al. (2008a)
Mg#91	P							
Ringwoodite								
Mg#90	SP?	20	1,073–1,473	2.92(4)	1.16(1)			Xu et al. (1998a)
Mg#90	P	20		3.61	1.08(2)		0.69(3)	Huang et al. (2005)
Mg#91	SP	20	500–1,700	2.92	1.36(5)			Yoshino et al. (2008a)
Mg#91	P	20	500–1,700	1.44	1.12(3)	0.67(3)		
Mg#91	SP	20	1,150–1,400	3.30(3)	0.92(0)			Yoshino and Katsura (2009)
Mg#80	SP	20	1,200–1,900	3.45(4)	1.26(1)			
Mg#70	SP	20	900–1,600	3.31(1)	1.44(0)			

Table 4 High-pressure electrical conductivities of garnet given in the Eq. 3

Composition	P (GPa)	T (K)	$\log\sigma_0$ (S/m)	ΔH((eV)	Reference
SCOPX[a]	21	1,473–1,773	3.35	1.66(3)	Xu and Shankland (1999)
Py100	10	1,573–1,973	2.67	2.56	Romano et al. (2006)
Py85Alm15	10	1,323–1,823	2.42	1.50	
Py60Alm40	10	973–1,673	3.14	1.26	
Py40Alm60	10	873–1,273	2.81	0.67	
Py20Alm80	10	573–873	3.34	0.56	
Alm100	10	573–873	4.39	0.68	
Py100	19	1,173–1,923	0.41	0.57	
Py85Alm15	19	1,173–1,923	1.52	0.91	
Py60Alm40	19	1,173–1,813	2.19	0.89	
PYR-OL	18	1,000–1,500	2.53	1.37	Yoshino et al. (2008b)
		1,600–1,900	3.44	1.63	
MORB[b]	18	700–2,000	3.10	1.38	

SCOPX San Carlos orthopyroxene with 2.89 wt.% Al_2O_3, *PYR-OL* Garnet composition with pyrolite minus olivine; *MORB* Mid-ocean ridge basaltic composition

Table 5 High-pressure electrical conductivities of silicate perovskite given in the Eq. 3

Composition	P (GPa)	T (K)	logσ (S/m)	ΔH(eV) ΔV(cm^3/mol)	References
DAC					
Mg# 89	40	298–571		~0.35	Peyronneau and Poirier (1989)
Mg# 92	40	298–571		~0.35	
Mg# 89	1.2–40	293–673	1.92(68)	0.48(2) −0.26(3)	Shankland et al. (1993)
KMA					
Al-free					
Mg# 93	23	400–900	0.60	0.41	Katsura et al. (1998)
		1,500–2,000	2.30	0.92	
Mg# 91.5	25	1,673–1,873	1.12(12)	0.62(4)	Xu et al. (1998b)
Mg# 90	25	350–1,100	0.91(2)	0.46(0)	Yoshino et al. (2008c)
		1,750–2,000	2.64(6)	0.93(2)	
Al-bearing (2.8 wt.%)					
Mg# 91.5	25	1,673–1,873	1.87(11)	0.70(4)	Xu et al. (1998b)
Mg# 92	25	373–923	ND	0.51(1)	Xu and McCammon (2002)
		1,612–1,971	3.45(24)	1.43(8)	
Na-bearing					
Mg# 100	24	1,300–1,800	3.92(3)	1.40(20)	Dobson (2003)
		1,800–2,200	9.40(40)	3.60(20)	

Omura (1991) firstly performed high-pressure conductivity measurements in a KMA and reported relatively higher conductivity values compared with the previous results determined at atmospheric pressure. These results have been debated on the basis of experimental complications such as no control of oxygen buffer and a presence of reaction products (Duba and von der Gönna 1994). Later, Xu et al. (1998a) improved experimental design and reported electrical conductivity of olivine under various pressure conditions (4, 7 and 10 GPa) and a temperature range from 1,273 to 1,673 K. The conductivity values are consistent with results at room pressure. Activation enthalpy is around 1.7 eV. In a wide pressure range (4–10 GPa), the electrical conduction slightly decreases with increasing pressure, and it has a positive activation volume of 0.68 cm^3/mol (Xu et al. 2000a, b). They proposed that small polaron conduction is a dominant conduction mechanism. However, a positive activation volume for small polaron conduction has not been reported for other ferromagnesian silicate minerals. Recently, Yoshino et al. (2009) identified three conduction mechanisms based on the conductivity measurements at a pressure of 10 GPa and temperatures up to 2000 K (Fig. 14a). They demonstrated that the conduction mechanism changes from small polaron to ionic conduction with temperature around 1,600 K, which is consistent with the experimental results at room pressure (Schock et al. 1989). For natural olivine with Mg/(Mg + Fe) = 91, the activation energy of ionic conduction (4.2 eV) is much higher than that of small polaron conduction (1.6 eV). At low temperatures, proton conduction with low activation energy (<1 eV) appears.

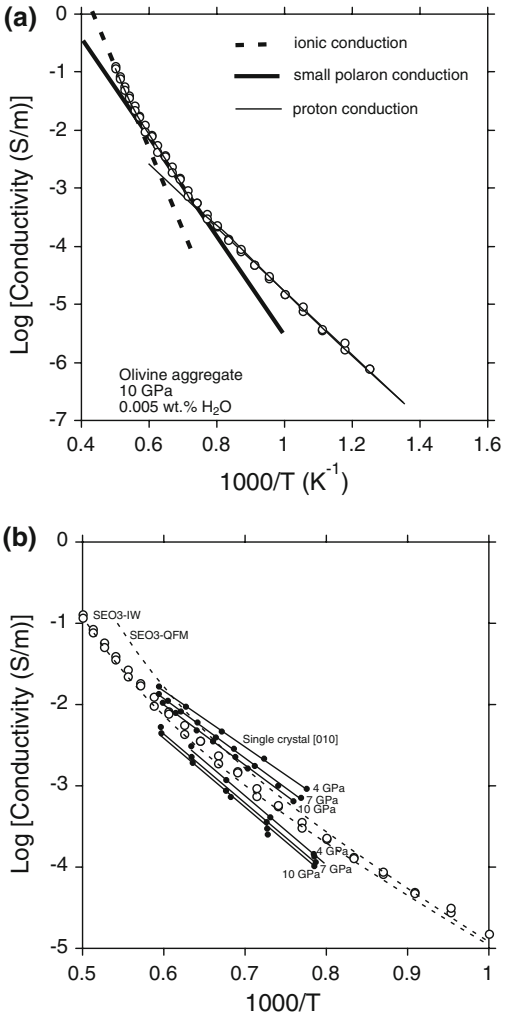

Fig. 14 Electrical conductivity of olivine as a function of reciprocal temperature. **a** Electrical conductivity of San Carlos olivine aggregates measured at 10 GPa (Yoshino et al. 2009). Note that three conduction mechanisms can be identified. The *dashed*, *solid thick* and *solid thin lines* indicate the estimated ionic, small polaron and proton conduction mechanisms, respectively. **b** Electrical conductivity data of olivine measured under high-pressure conditions. *Open circles* indicate 10 GPa data from Yoshino et al. (2009). *Closed diamonds* and *circles* indicate single crystal data [010] from Xu et al. (1998a) and polycrystal data from Xu et al. (2000a, b), respectively. *Short* and *long dashed lines* represent C06: the latest model of olivine electrical conductivity at 0.1 MPa under QFM (quartz-fayalite-magnetite) and IW (iron-wüstite) buffers, respectively, from Constable (2006)

Two inconsistent experimental reports on proton conduction in olivine were recently published in the same issue of Nature (Yoshino et al. 2006; Wang et al. 2006). Figure 15 shows conductivity data of hydrous olivine. Based on the conductivity measurement of the single crystal of relatively dry and hydrous olivine, Yoshino et al. (2006) reported that although the presence of water enhances the electrical conductivity of olivine, this effect is not large enough to explain the high conductivity at the top of the asthenosphere. In contrast, Wang et al. (2006) reported that hydrous olivine showed much higher conductivity and a larger temperature dependence than those with the similar water content from the study of Yoshino et al. (2006). As a result, Wang et al. (2006) concluded that the hydrous olivine is responsible for the high conductivity at the top of the asthenosphere. A cause of this discrepancy was discussed in the former chapter (3.5).

Important results obtained from Yoshino et al. (2006) are as follows: (1) lower activation energy for proton conduction (0.7–0.9 eV), (2) small contribution of proton conduction at high temperatures, and (3) weak anisotropy for proton conduction at high

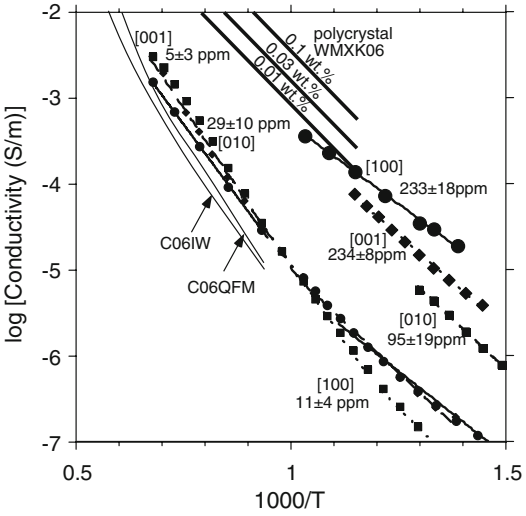

Fig. 15 Electrical conductivity of hydrous olivine as a function of reciprocal temperature. Each data points represents raw conductivity data of single crystal olivine from Yoshino et al. (2008a). *Numbers* indicate crystallographic orientation and H_2O in weight ppm in olivine single crystal. WMXK06: Wang et al. (2006). *Thin solid lines* represent C06: the latest model of olivine electrical conductivity at 0.1 MPa under QFM (quartz-fayalite-magnetite) and IW (iron-wüstite) buffers from Constable (2006)

temperatures. Although Karato (1990) predicted high conductivity values for proton conduction based on the hydrogen diffusion data of olivine, the conductivity values and activation energy for proton conduction is much smaller compared to that for the hydrogen diffusion (1.14–1.86 eV) (e.g., Mackwell and Kohlstedt 1990). This inconsistency would be derived from a difference of the initial conditions; initially dry for hydrogen diffusion experiment and homogeneous hydrogen content in olivine for conductivity measurement. For the hydrogen diffusion experiments, the migration of protons must be accompanied by the creation of vacancy to establish charge balance within the olivine crystal. The resultant activation enthalpy for hydrogen diffusion into the hydrogen-free crystal would become higher. Mackwell and Kohlstedt (1990) also reported one order of magnitude high diffusion rate for the [100] direction compared with the other crystallographic directions at high temperatures. However, the conductivity data showing isotropic features at high temperatures are consistent with a little difference of diffusion rate for each crystallographic direction for dehydration experiments of hydrous olivine by Kohlstedt and Mackwell (1998).

4.2 Wadsleyite and Ringwoodite

Wadsleyite and ringwoodite are the main constituent minerals in the mantle transition zone (410–660 km depth), and can store a significant amount of water in their crystal structure. Figure 16 shows electrical conductivity data of wadsleyite and ringwoodite as a function of water content. Xu et al. (1998a) reported that electrical conductivities of wadsleyite and ringwoodite are similar and two orders of magnitude higher than that of olivine. However, their conductive values are too high to explain the recent conductivity-depth profiles in the transition zone obtained by the semi-global electromagnetic induction studies (e.g., Neal et al. 2000; Tarits et al. 2004; Kuvshinov et al. 2005). Later, although Xu et al. (1998a) considered that the dominant conduction mechanisms in their study are small polaron, Huang et al. (2005) attributed the results of Xu et al. (1998a) to proton conduction because they found a significant amount of water in Xu et al.'s samples. This means that we have no data about the small polaron conductions of these minerals. Although Huang et al. (2005)

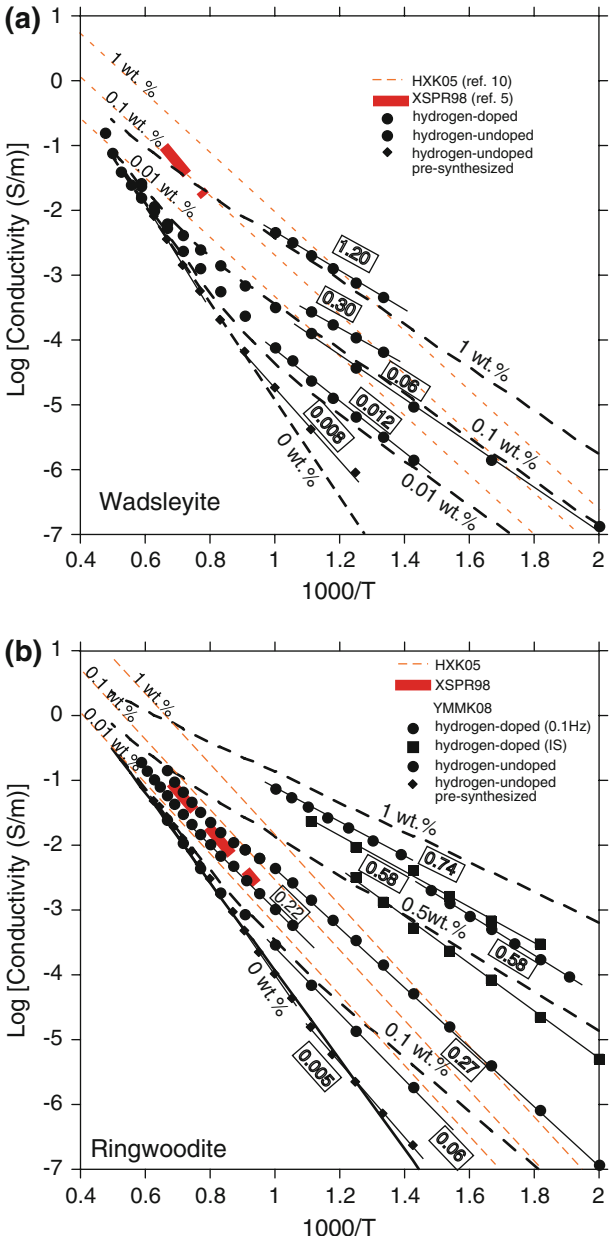

Fig. 16 Electrical conductivity of wadsleyite and ringwoodite as a function of reciprocal temperature. The *symbols* indicate raw data for each sample with different water contents from YMMK08 (Yoshino et al. 2008a). *Open diamonds*, *open circles* and *closed circles* indicate results for the pre-synthesized (undoped), the hydrogen undoped and the hydrogen doped samples, respectively. *Very thick red* and *thin orange dashed lines* represent experimental results from XSPR98 (Xu et al. 1998a) and HXK05 (Huang et al. 2005) as a function of water content, respectively. *Thick dashed lines* indicate the electrical conductivity calculated by data fitting based on the equation, $\sigma = \sigma_{0H}\exp\left(-\frac{H_H}{kT}\right) + \sigma_{0P}C_w\exp\left(-\frac{H_P^0 - \alpha C_w^{1/3}}{kT}\right)$ (18) as a function of water content. *Numbered boxes* denote the estimated water content (in weight percent) by FT-IR analysis. Errors for the estimated water content become larger with decreasing water content and range from ±20 (~1 wt.%) to ± 50% (<0.01 wt.%)

claimed that they determined proton conduction of these minerals, their results can be considered invalid because of serious methodological problems as described in the former chapter.

Yoshino et al. (2008a) distinguished between small polaron and proton conduction mechanisms of wadsleyite and ringwoodite by means of the conductivity measurement in a wider temperature range. The important features obtained from their study are as follows;

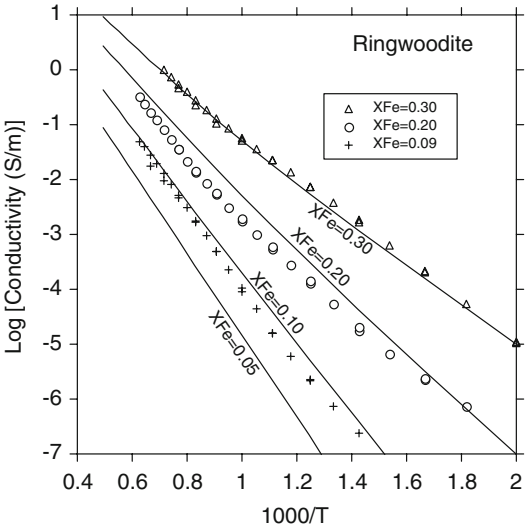

Fig. 17 Electrical conductivity of iron-bearing ringwoodite as a function of total iron content for several temperatures (Yoshino and Katsura 2009). *Symbols* denote the measured electrical conductivity. *Solid lines* indicate electrical conductivity of various iron content calculated from Eq. 11 as a summation of electrical conductivities of low and high temperature regimes

(1) Electrical conductivity of ringwoodite is around one magnitude higher than that of wadsleyite, (2) Conductivity values and activation energy for proton conduction increase with increasing water content, (3) Small polaron conduction becomes dominant at high temperatures. These features are quite same as olivine. Dominant conduction mechanism at the mantle temperature condition is small polaron mobility (1.49 eV for wadsleyite; 1.36 eV for ringwoodite).

Figure 17 shows effect of total iron content ($Fe^{2+} + Fe^{3+}$) on electrical conductivity of ringwoodite under the same oxygen buffer (Mo–MoO_2) (Yoshino and Katsura 2009). The conductivity largely increases with increasing total iron content. The activation energy becomes higher at a certain temperature. At high temperatures, the activation energy decreased from 1.44 to 0.92 eV with increasing total Fe content. At low temperatures less than 1,000 K, the activation energy also decreases from 1.15 to 0.74 eV with total Fe content. This behavior of activation energy can be expressed by n type semiconductor model [Eq. 11]. Dependence of the activation energy on Fe content suggests that the dominant mechanism of charge transport is Fe^{2+}–Fe^{3+} hopping (small polaron).

4.3 Garnet (Majorite)

Garnet is a stable phase over a wide range of pressure conditions from the Earth's crust down to the upper part of the lower mantle. In the depth range from 300 to 500 km (depending upon the bulk composition), pyroxenes progressively dissolve into garnet with increasing pressure, forming majorite (e.g., Takahashi and Ito 1987; Irifune and Ringwood 1993). Majoritic garnet is the second abundant mineral in the transition zone for a pyrolite composition. Furthermore, majoritic garnet is the most abundant mineral in the basaltic layer of subducted lithosphere in the mantle transition zone (410–660 km depth) (e.g. Irifune et al. 1986; Irifune and Ringwood 1993; Hirose et al. 1999; Ono et al. 2001). The volume proportion of majorite in the primitive MORB is close to $\sim$90% in volume.

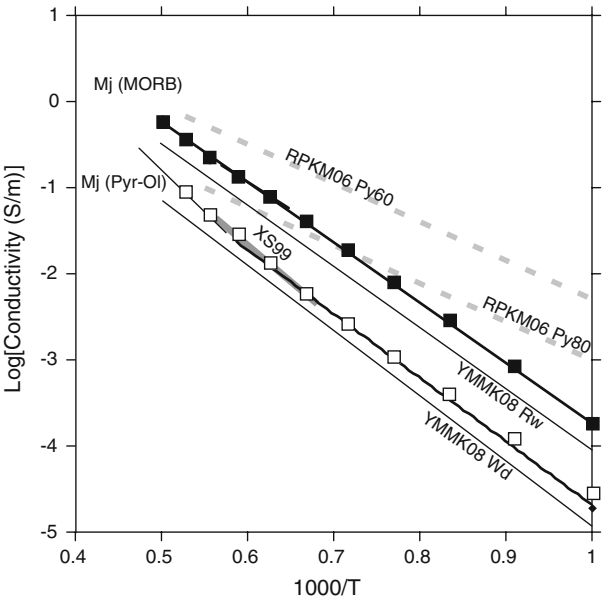

Fig. 18 Logarithm of electrical conductivity versus reciprocal temperature for majorite garnet. *Symbols* indicate data from pyrolite majorite (*open squares*) and MORB majorite (*closed squares*) (Yoshino et al. 2008b). *Shaded line* indicates the Arrhenius plot of ilmenite + garnet polycrystals (Xu and Shankland 1999). *Shaded dashed lines* denote the Arrhenius plot of garnets in almandine-pyrope solid solution (py60 and py80) determined at 19GPa (Romano et al. 2006). *Thin black lines* denote the Arrhenius plot of dry wadsleyite and ringwoodite polycrystals from our data (Yoshino et al. 2008a)

Figure 18 shows electrical conductivity data of garnets with various chemical compositions. Xu and Shankland (1999) firstly measured electrical conductivity of garnet using orthopyroxene containing 2.89% Al_2O_3 by weight as a starting material under the pressure condition of the mantle transition zone. However, the recovered sample was a mixture of ilmenite and garnet. Romano et al. (2006) reported the electrical conductivity of garnet as a function of iron content ($Fe_3Al_2Si_3O_{12}$–$Mg_3Al_2Si_3O_{12}$ join) at pressures from 10 to 19 GPa. At 10 GPa, activation energies for conductivity vary smoothly with composition and increase rapidly toward the pyrope ($Mg_3Al_2Si_3O_{12}$) end-member composition, suggesting that small polaron conduction is favorable mechanism. At 19 GPa, however, there is virtually no change in the activation energy as a function of Fe–Mg substitution for the pyrope-rich garnets. No dependence of iron content on activation energy was interpreted by a mechanism involving oxygen related point defects. Yoshino et al. (2008b) measured electrical conductivities of majorite garnet with compositions of pyrolite minus olivine (pyrolite majorite) and mid-ocean ridge basalt (MORB majorite) at 18 and 23 GPa and temperatures up to 2,000 K. To evaluate electrical conductivity of the mantle transition zone, chemical composition of garnet with pyrolite minus olivine is the most suitable (see Fig. 1). The conductivity of the MORB majorite (high Fe/(Fe + Mg) and Al-rich) is more than twice higher than those of the pyrolite majorite at the same temperature. The activation energies of these majorites are both 1.4 eV at temperature of 1,000 to 1,600 K, suggesting that the dominant mechanism of charge transportation is small polaron conduction. Small dependence of activation enthalpy on Fe/(Fe + Mg) would be caused by more complex solid solution of majorite-pyrope join compared to a simple solid solution of pyrope-almandine join due to the Fe–Mg exchange. At higher temperatures (>1,600 K), activation enthalpy of the pyrorite majorite becomes higher. Yoshino et al. (2008b) interpreted that the conduction mechanism of the pyrolite majorite changes from small polaron to ionic conduction. The pyrolite majorite has only slightly higher and lower conductivity than dry wadsleyite and ringwoodite (Yoshino et al. 2008a), respectively, and

will not largely change the conductivity-depth profile predicted from the electrical conductivities of wadsleyite and ringwoodite.

4.4 Silicate Perovskite

Silicate perovskite is thought to be the major phase in the Earth's lower mantle and to store much of aluminum and iron in the lower mantle (Ito and Takahashi 1991; Wood and Rubie 1996). Electrical conductivity of silicate perovskite has been firstly measured in DAC (Peyronneau and Poirier 1989; Li and Jeanloz 1990a; Shankland et al. 1993). Poirier's group conducted the conductivity measurement under low temperature conditions (<700 K) using external heating system (Peyronneau and Poirier 1989; Shankland et al. 1993), whereas Li and Jeanloz (1990a) used laser-heating system to establish the physical conditions of the lower mantle. Shankland et al. (1993) reported activation energy of 0.4 eV and activation volume of -0.1 to -0.3 cm^3 mol^{-1} in a temperature range from 293 to 673 K and at pressures of 1.2 and 40 GPa. This small negative activation volume is consistent with a conduction mechanism in which charge is carried by electrons hopping from Fe^{2+} and Fe^{3+} ions (small polaron). They estimated the maximum conductivity value of 3–10 S/m at the base of the lower mantle based on the extrapolation of low temperature data to the mantle condition. On the other hand, Li and Jeanloz (1990a) reported extremely lower conductivity values ($\sim 10^{-4}$ S/m) at temperature above 2,000 K compared with the geophysical observations (e.g., Egbert and Brooker 1982). The low conductivity values obtained from Li and Jeanloz (1990a) are probably due to no control of oxygen fugacity and large temperature gradient in a laser heated diamond anvil cell. Because of experimental limitations of temperatures and pressures, extrapolation of laboratory data to mantle conditions has been unavoidable.

In the end of 1990s, two groups performed conductivity measurements of the silicate perovskite in a Kawai-type multi-anvil press under the physical conditions of the uppermost lower mantle (Katsura et al. 1998; Xu et al. 1998b). Katsura et al. (1998) identified two different activation energies at low and high temperatures. The activation energy for the low temperature region is in good agreement with that reported by Shankland et al. (1993), who also measured the conductivity of quenched perovskite at similar temperatures. However, at high temperatures above 1,500 K, activation energy becomes distinctly high (0.92 eV). Xu et al. (1998b) also reported slightly higher activation energy (0.62 eV) at high temperature region than the previous works (Peyronneau and Poirier 1989; Shankland et al. 1993). These studies suggested that the electrical conductivity of perovskite must be measured in its stability field in order to make direct comparisons with the conductivity of the lower mantle. $(Mg,Fe)SiO_3$ perovskite has slightly higher conductivity than ringwoodite with the same Mg#. The absolute values of both groups are similar, but the activation energies of 0.62 eV for conduction in perovskite obtained by Xu et al. (1998b) are lower than the value of 0.92 eV determined from high temperature data of Katsura et al. (1998). A recent conductivity measurement of $(Mg_{0.9},Fe_{0.1})SiO_3$ perovskite in a continuous wide temperature range from 300 to 2,000 K showed a change of activation energy from 0.46 to 0.93 eV (Yoshino et al. 2008c). This tendency is in agreement with the results of Katsura et al. (1998). In this study, high activation energy appears around 1,700 K.

A presence of impurities in perovskite profoundly affects the electrical conductivity of silicate perovskite (Fig. 19). Xu et al. (1998b) reported a significant effect of aluminum on the conductivity of perovskite. Perovskite containing 2.89 wt.% Al_2O_3 is about 3.5 times greater than that of aluminum-free perovskite. The conduction mechanism in perovskite

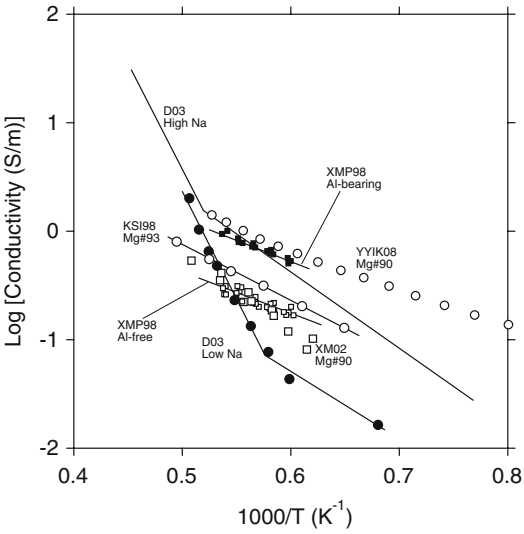

Fig. 19 Effect of impurities on electrical conductivity of silicate perovskite. *KSI98* Katsura et al. (1998), *XSPR98* Xu et al. (1998b), *XM02* Xu and McCammon (2002), *D03* Dobson (2003), *YYIK08* Yoshino et al. (2008c)

has been interpreted by small polaron conduction, because the aluminum-bearing perovskite has about 3.5 times the amount of Fe^{3+} as the aluminum-free sample. Aluminum incorporation into the perovskite structure leads to higher Fe^{3+} concentration due to the charge couple substitution even if the oxygen fugacity is low (McCammon 1997, 2005). Later, Xu and McCammon (2002) reported evidence that in aluminous perovskite with Mg#90, ionic conduction characterized by high activation energy ($\sim$1.5 eV) becomes significant above 1,700 K. This is most likely due to the presence of oxygen vacancies, which charge-balance Al substituting onto the Si-site (Brodholt 2000; Lauterbach et al. 2000). To investigate electric conduction due to the migration of oxygen vacancy, Dobson (2003) measured the electrical conductivity of Na-doped $MgSiO_3$ perovskites at 24 GPa and temperatures between 1,300 and 2,200 K. Activation energy changes from 1.4 $\pm$ 0.2 to 3.6 $\pm$ 0.2 eV with increasing temperature around 1,800 K. At low temperatures below 1,800 K, the dominant conduction mechanism was interpreted as extrinsic oxygen ionic conduction based on the observation that a pre-exponential is proportional to the Na-content. If perovskite with a natural composition contains a significant extrinsic oxygen vacancy content (Lauterbach et al. 2000), oxygen ionic conduction might dominate in the lower mantle. At higher temperatures, a different conduction mechanism, which is insensitive to Na-content, dominates with $\Delta H = 3.6 \pm 0.2$ eV and $\log \sigma_0 = 9.4 \pm 0.4$ S/m. This anomalously high activation energy has not been observed in the other studies.

Lower mantle pressures increase from 23 GPa at the 660 km seismic discontinuity to 136 GPa at the core-mantle boundary. Above 30 GPa, electrical conductivity measurement has been conducted in a diamond anvil cell equipped with laser heating system. Recently Ohta et al. (2008) reported that electrical conductivity of perovskite with a composition of $(Mg_{0.9}Fe_{0.1})SiO_3$ decreases with pressure due to high-spin to low-spin transition of iron in perovskite (Fig. 20). Spin transition pressure of perovskite phase is in still debate. Based on X-ray emission study, Badro et al. (2004) reported a two step transition at $\sim$70 GPa for Fe^{2+} and $\sim$120 GPa for Fe^{3+} in $(Mg_{0.9}Fe_{0.1})SiO_3$, whereas Li et al. (2004) suggested that the transition occurs gradually with increasing pressures in aluminum bearing perovskite. According to the theoretical works (e.g., Lin et al. 2005), the spin transition pressures in

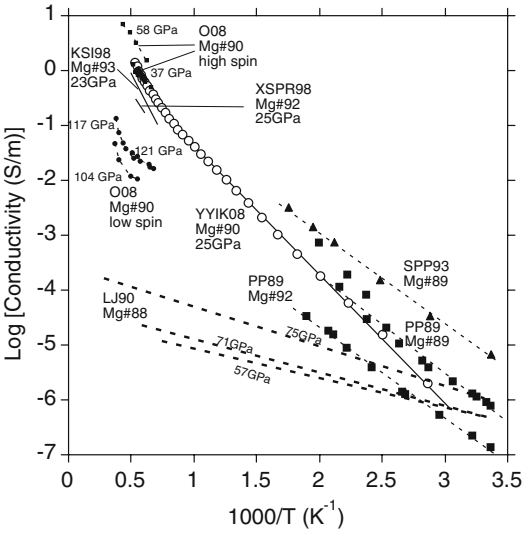

Fig. 20 Logarithm of electrical conductivity versus reciprocal temperature for Al-free silicate perovskite. *Open* and *closed symbols* or *solid* and *dotted lines* indicate data obtained from the DAC and the KMA, respectively. *PP89* Peyronneau and Poirier (1989), *LJ90* Li and Jeanloz (1990), *KSI98* Katsura et al. (1998), *XSPR98* Xu et al. (1998b), *O08* Ohta et al. (2008), *YYIK08* Yoshino et al. (2008c)

perovskite varies for ferric and ferrous irons; ferric iron shows a wide pressure interval of spin transition between about 60–160 GPa, whereas ferrous iron is in a high spin state at all mantle pressures and it transforms to the low spin state at pressures about 130–145 GPa. These theoretical and experimental results revealed a pressure-induced gradual loss of magnetic moment in an aluminum bearing perovskite sample between 20 and 100 GPa, indicating possible occurrence of mixed spin state and intermediate-spin state under high pressures to 100 GPa in aluminum bearing perovskite.

4.5 Ferropericlase

Ferropericlase (Mg,Fe)O is the second abundant mineral in the lower mantle, and is a solid solution between periclase (MgO), a wide band gap insulator, and wüstite (FeO), a classical Mott insulator. Figure 21 shows electrical conductivities of ferro-periclase in Arrehenius plot. The conductivity measurements of ferro-periclase have been performed separately at high (>1,300 K) and low (<1,000 K) temperatures. Wood and Nell (1991) demonstrated that electrical conductivity of ferro-periclase with Mg# 83 at atmospheric pressure is largely higher than that of co-existing silicate perovskite. Li and Jeanloz (1990b) performed the conductivity measurement under unbuffered condition in the DAC at higher pressures ($\sim$30 GPa). This DAC study used external (<500 K) and laser (>1,500 K) heating. In general, high temperature part is characterized by higher activation energy. However, absence of conductivity data in the intermediate temperature range yielded a break in slope in Arrhenius plot. Dobson et al. (1997) and Dobson and Brodholt (2000) firmly confirmed a change of activation energy between low and high temperature measurements using the KMA based on the conductivity measurement under a continuous change of temperature. At low temperatures, electronic hopping between Fe^{2+} and Fe^{3+} (small polaron) with activation enthalpies of 0.37 eV is dominant conduction mechanism, and a positive dependence of σ_0 on Fe/(Fe + Mg) has been observed. Activation energies become higher at around 1,000 K. At high temperatures (>1,000 K), large polaron conduction appears (Dobson et al. 1997). The activation energy for large polaron conduction

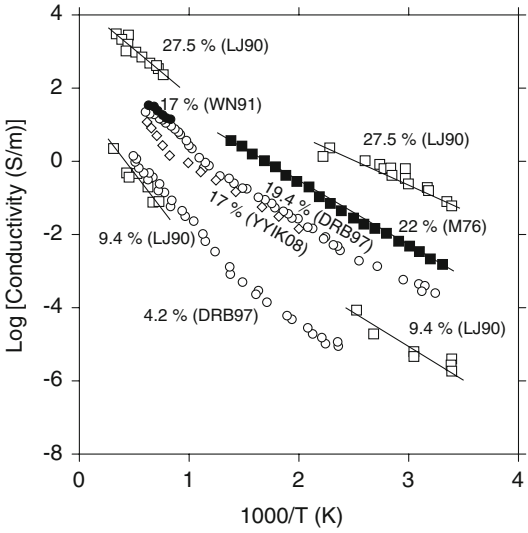

Fig. 21 Logarithm of electrical conductivity versus reciprocal temperature for ferro-periclase under high pressure. *M76* Mao (1973) measured at 30 GPa, *LJ90* Li and Jeanloz (1990) measured at 30 GPa, *WN91* Wood and Nell (1991) measured at room pressure, *DRB97* Dobson et al. (1997) measure at 5 GPa, *YYIK08* Yoshino et al. (2008c) measured at 25 GPa

increases with decreasing total iron content, ranging from 0.4 to 1.1 eV. At temperatures corresponding to the lower mantle, the dominant conduction mechanism is probably large polaron process.

In the Al-free peridotite, iron preferentially partition into ferropericlase in comparison with the silicate perovskite (e.g., Katsura and Ito 1996). Thus high iron content in ferropericlase phase leads to higher conductivity than silicate perovskite. Even though silicate perovskite is volumetrically major phase in the lower mantle rocks, if ferropericlase is interconnected in lower mantle rocks, the lower mantle conductivity could be higher than that expected from the silicate perovskite (Wood and Nell 1990). To investigate interconnectivity of ferropericlase in silicate perovskite matrix, Yoshino et al. (2008c) measured electrical conductivities of post-spinel (silicate perovskite 68 vol.% and ferropericlase 32 vol.%) with a bulk composition of $((Mg,Fe)_2SiO_4$: $X_{Fe} = 0.09)$, which are thought to be a dominant assembly in the lower mantle. Figure 22 shows a comparison of electrical conductivities between silicate-perovskite, ferro-periclase and post-spinel phase at the same pressure condition (25 GPa). Both absolute values and change in activation enthalpy for the conductivity of the post-spinel phases are quite similar to those for the silicate perovskite. These observations suggest that ferro-periclase in post-spinel are isolated in silicate perovskite matrix. Volume fraction of ferro-periclase in the pyrolitic mantle is around 18 vol.%, which is lower than that of postspinel. Interconnection of ferropericlase is more difficult to establish in the lower mantle rocks. As a result, the conductivity of silicate-perovskite can mostly control the electrical conductivity structure of the lower mantle.

Badro et al. (2003) firstly showed that ferro-periclase undergoes a spin transition at pressures above 60 GPa. The high-spin to low-spin transition in (Mg, Fe)O ferropericlase at high pressure has been confirmed by many recent studies including X-ray emission spectroscopic measurements (Lin et al. 2005), conventional and synchrotron Mössbauer spectroscopic studies (Keppler et al. 2007), and theoretical calculations (Sturhahn et al. 2005; Persson et al. 2006; Tsuchiya et al. 2006). In the lower mantle, electrical conductivity of ferropericlase is possible to change in association with a difference of band gap

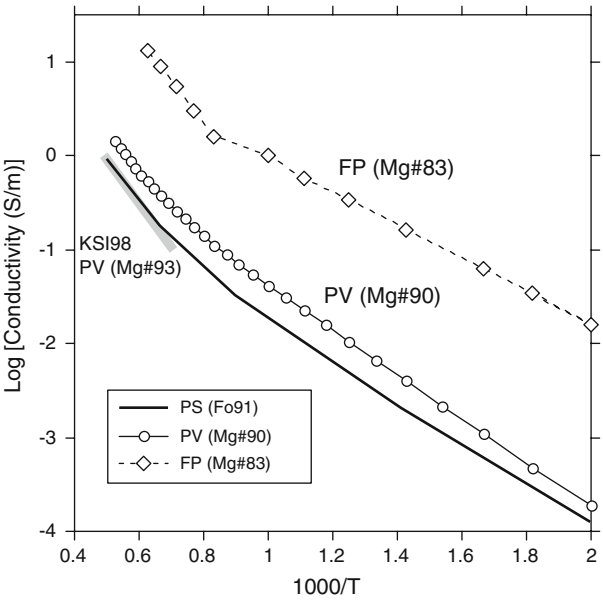

Fig. 22 Logarithm of electrical conductivity versus reciprocal temperature for post-spinel, ferro-periclase (Mg# 83) and silicate perovskite (Mg# 90) from Yoshino et al. (2008c). *Thin shaded line* denotes the Arrhenius plot of silicate perovskite with Mg# 93 from Katsura et al. (1998). Since magnesium number (Mg#) of silicate perovskite in post-spinel is around 95, the conductivity of the silicate perovskite coexisting with ferro-periclase is expected to be much lower than data of Katsura et al. (1998)

structure due to the spin transition. Lin et al. (2007a) measured electrical conductivity of the ferropericlase $(Mg_{0.75},Fe_{0.25})O$ using diamond anvils to pressures over 100 GPa at low temperatures up to 500 K. The electrical conductivity gradually increases by an order of magnitude up to 50 GPa but decreases by a factor of approximately three between 50 and 70 GPa. Ohta et al. (2007) reported electrical conductivity of the ferropericlase $(Mg_{0.81},Fe_{0.19})O$ using diamond anvils to pressures up to 135 GPa at room temperature (300 K). Although the absolute conductivity values are largely different from each other due to usage of samples with different iron content, a trend showing a gradual decrease of electrical conductivity between 50 and 80 GPa is quite consistent as shown in Fig. 23. This decrease in the electrical conductivity has been interpreted by the isosymmetric high-spin to low-spin transition of iron in ferropericlase. The electronic spin transition of iron would result in a decrease in the mobility and/or density of the charge transfer carriers in the low-spin ferropericlase. The activation energy of the low-spin ferropericlase (0.27 eV at 101 GPa) was considered as the small polaron conduction (Lin et al. 2007a). They concluded that low-spin ferropericlase exhibits lower electrical conductivity than high-spin ferropericlase. However, if the dominant conduction mechanism at high temperatures was different from small polaron (Dobson et al. 1997), simple extrapolation of their data to high temperatures is dangerous. On the other hand, recent theoretical calculations predict that the spin transition of Fe^{2+} in ferropericlase, $(Mg_{1-x}Fe_x)O$ ($x < 0.2$), would occur continuously over an extended pressure range under the pressure–temperature conditions of the lower mantle (Sturhahn et al. 2005; Tsuchiya et al. 2006). Recent experiments confirmed that a gradual spin transition of iron occurs over a wide pressure–temperature range in the lower mantle (Lin et al. 2007b). As a transition pressure range from high to low spin tends to expand with increasing temperature, it would be difficult to detect the discontinuity of conductivity structure from the electromagnetic observations. In future, it is needed to investigate effect of a spin transition on electrical conductivity of ferro-periclase at temperatures corresponding to the lower mantle.

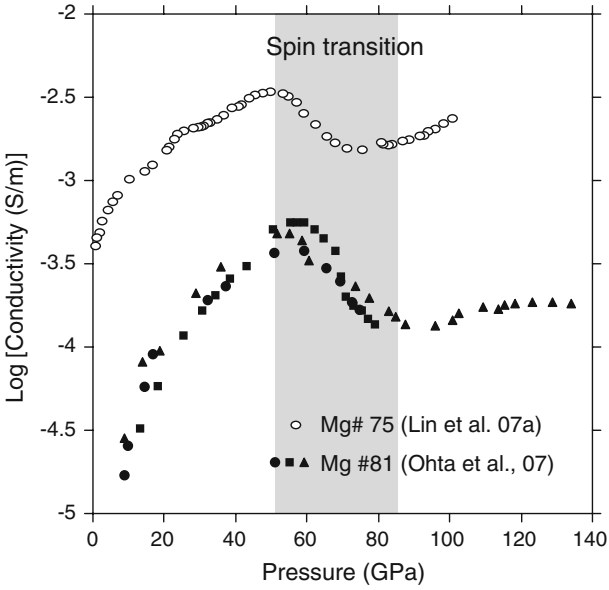

Fig. 23 Effect of spin-transition on electrical conductivity of ferro-periclase at room temperature. Data points are from Lin et al. (2007a) and Ohta et al. (2007)

4.6 Silicate Post-Perovskite

Large seismic anomalies have been observed at the bottom of lower mantle with a thickness of several hundreds kilometers (D" layer) (e.g., Lay and Helmberger 1983; Lay et al. 1998). The anomalies of the D" layer are difficult to explain with known physical properties of $MgSiO_3$ perovskite—the main constituent of the lower mantle. The recent discovery of the $MgSiO_3$ post-perovskite phase transition has provided new insights into the D" layer from high-pressure experiments with the diamond anvil cell (DAC) (Murakmi et al. 2004). The transition pressure of $MgSiO_3$ perovskite to post-perovskite (125 GPa) is consistent with the depth of the velocity increase at the D" seismic discontinuity (2,700 km depth) (Lay et al. 1998). In order to understand the mantle dynamics near the core-mantle boundary, the physical properties of the post-perovskite phase have been determined by many researchers.

A first report on electrical conductivity of silicate post-perovskite with a composition of $(Mg_{0.89}Fe_{0.11})SiO_3$ and $Fe^{3+}/(Fe^{2+} + Fe^{3+})$ of 0.13 ± 0.10 at 129 and 143 GPa using LH-DAC showed extremely high conductivity ($>10^2$ S/m) in comparison with that of silicate perovskite and little temperature dependence at the conditions of D" layer (Ohta et al. 2008). Because the post-perovskite phase with a $CaIrO_3$ structure has a stacked SiO_6-octahedral sheet structure with interlayer (Mg, Fe) ions (Murakmi et al. 2004), Ohta et al. (2008) interpreted that the high conductivity likely reflects the short Fe–Fe hopping distance in the (Mg, Fe) layer, which is shorter than that in perovskite. They reported a little positive dependence of electrical conductivity on temperature at a fixed pressure determined at room temperature. Pressure should increase during heating due to the thermal expansion of samples. If the electrical conductivity of the post-perovskite has positive pressure dependence, temperature may have a small negative effect, suggesting metallization. Further studies including the effect of Al and Fe contents on the electrical conductivity of the post-perovskite phase are needed to characterize the conductivity structure near the core-mantle boundary.

5 Geophysical Applications

5.1 Conductivity-Depth Profile

The electrical conductivity profile in the mantle has been obtained by electromagnetic induction studies. The penetration depths of electromagnetic fields within the Earth depend on the electromagnetic sounding period. The maximum penetration depths that can be routinely achieved using magnetotellurics (MT) sounding are of the order 400–600 km. It has been difficult to accurately determine the conductivity structure at the depth of mantle transition zone. Recently the conductivity-depth profile in the oceanic area has been improved by long-period electromagnetic observations, using the variations of voltage difference measured in unpowered submarine telecommunications cables (e.g., Lizarralde et al. 1995; Utada et al. 2003; Kuvshinov et al. 2005). Nevertheless, the constructed conductivity-depth profiles are strongly influenced by the assumed model such as smooth model and 2-layer model for inversion of data. Although the conductivity-depth profiles obtained from the geophysical observations show significant differences from each other, the following features can be seen in the most conductivity model (Fig. 24). Conductivity generally increases with increasing depth to the top of the lower mantle from 10^{-3}–10^{-2} to 10^{0} S/m. In the upper mantle, some studies have shown that the electrical conductivity of the uppermost upper mantle to 100 km depth is about 10^{-2} to 10^{-1} S/m, known as the high conductive layer (e.g., Lizaralde et al. 1995; Evans et al. 2005). Local variations of electrical conductivity are large at shallow depths, and become smaller with depth.

Figure 25 shows that mantle minerals with a higher-pressure stability field generally have higher conductivity. This tendency can explain the increase of electrical conductivity in the mantle well. Because activation enthalpy for small polaron conduction is smaller for mantle minerals with higher-pressure stability field, as pressure increases the temperature dependence becomes smaller. For this reason, the uniform electrical conductivity is expected to be in the deeper mantle. However, the high to low spin transition in iron of

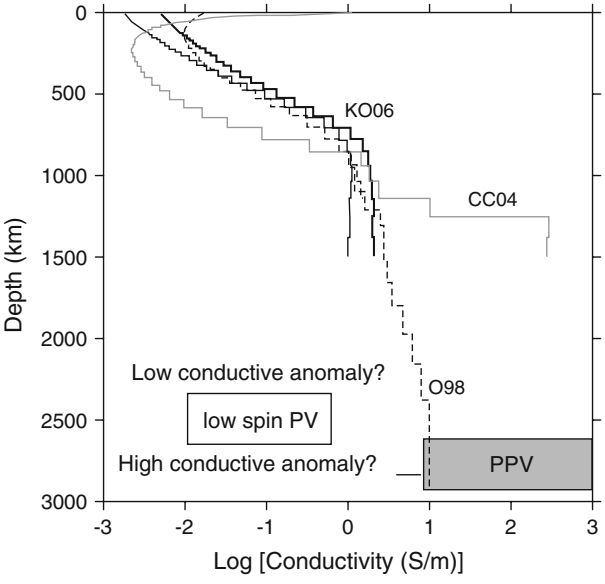

Fig. 24 1-D conductivity depth models based on the electromagnetic induction studies. *Dark shaded* and *light shaded* areas indicate possible presence of conductivity anomaly derived from the high to low spin transition of silicate perovskite and the perovskite to post-perovskite transition, respectively (Ohta et al. 2008). *O99* Olsen (1999), *CC04* Constable and Constable (2004), *KO06* Kuvshinov and Olsen (2006)

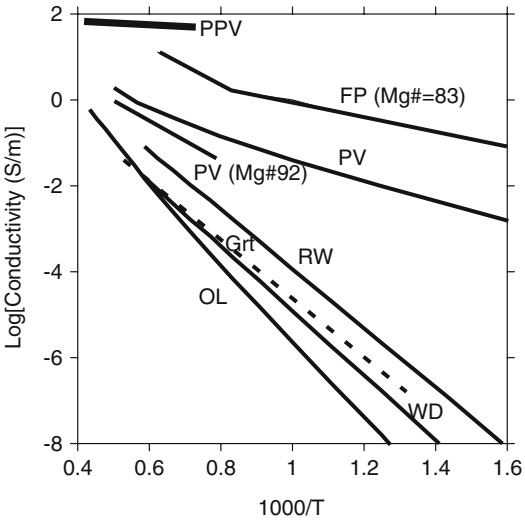

Fig. 25 Electrical conductivity of mantle minerals with Mg# = ~90; olivine (Yoshino et al. 2009), wadsleyite (Yoshino et al. 2008a), ringwoodite (Yoshino et al. 2008a), silicate perovskite (Al-PV) (Yoshino et al. 2008c), ferro-periclase (FP) (Yoshino et al. 2008c) and post-perovskite (PPV) (Ohta et al. 2008) in Arrhenius plot

silicate perovskite would yield lower conductivity in the deeper part of the lower mantle. On the other hand, D" layer composed of post-perovskite might be abnormally high conductive layer.

5.2 Conductivity Anomaly at the Top of the Asthenosphere

The conductivity of the high conductive layer at the top of the asthenosphere (60–100 km depth) is too high to be explained by the conductivity of ordinary anhydrous olivine. For example, Evans et al. (2005) reported that the oceanic asthenosphere has high electrical conductive region at 100 km depth, which is highly anisotropic in the Eastern Pacific Rise. One possibility is that partial melting occurs in the region and the melt forms an anisotropic interconnected conductive path in the partially molten peridotites. Another possibility is that olivine in the region contains considerable amounts of hydrogen inside crystal structure and thus the electrical conductivity is substantially raised by proton conduction (Karato 1990). Yoshino et al. (2006) reported the electrical conductivity of single crystal hydrous olivine, showing that conductivity of hydrous olivine at the top of the asthenosphere should be nearly isotropic and distinctly lower than that obtained from Evans et al. (2005). They concluded that the hydration of olivine cannot account for the geophysical observations, which instead may be explained by the presence of partial melt elongated in the direction of plate motion. Later, Gaillard et al. (2008) reported extremely high electrical conductivities of molten carbonates that are three orders of magnitude higher than those of molten silicate and five orders of magnitude higher than those of hydrated olivine. They proposed that high conductivities in the asthenosphere indicate the presence of small amounts of carbonate melt in peridotite.

5.3 Water in the Mantle Transition Zone

The Earth's mantle transition zone would be a large water storage because wadsleyite and ringwoodite can store significant amounts of water in their crystal structure (e.g., Kohlstedt et al. 1997). A laboratory based electrical conductivity model across the mantle transition

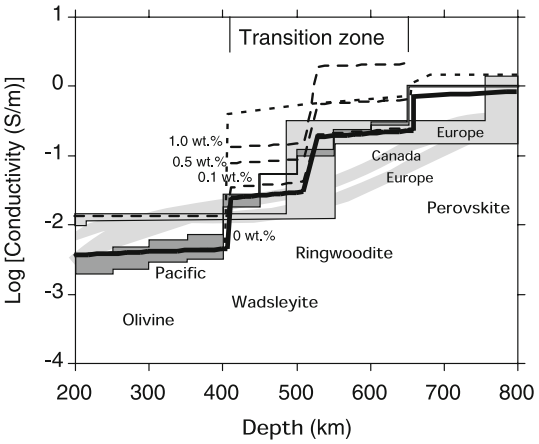

Fig. 26 The electrical conductivity profiles of the mantle across the transition zone. *Thick solid* and *dashed lines* indicate dry and wet mantle models by Yoshino et al. (2008a), respectively. *Thin dashed line* denotes laboratory conductivity model by Xu et al. (2000a, b). *Shaded areas* represent the conductivity-depth models obtained from the electromagnetic observations by Tarits et al. (2004): Europe; Olsen (1998): Europe; Neal et al. (2000): Canada; Kuvshinov et al. (2005): Pacific. An inversion model of Olsen (1998) assumed a conductivity jump at 500 km depth. The conductivity-depth profiles from Neal et al. (2000) and Tarits et al. (2004) are the inversion model without considering a conductivity jump. The models of Kuvshinov et al. (2005) present a range of conductivity with and without a conductivity discontinuity at 400 km depth

zone by Yoshino et al. (2008a) is shown with geophysical observations (Fig. 26). A recent semi-global reference model for electrical conductivity widely covers the mantle transition zone of the one-fourth of the Earth beneath the north Pacific Ocean (Utada et al. 2003; Kuvshinov et al. 2005). According to this model, the conductivity slightly jumps at the top of the mantle transition zone (410 km discontinuity) and gradually increases to the top of the lower mantle. The laboratory-based model by Xu et al. (2000a, b) showed a single large conductivity jump at 410 km discontinuity. However, most of the recent conductivity-depth models do not show such a distinct conductivity jump at this depth (e.g., Olsen 1998; Neal et al. 2000; Tarits et al. 2004). In addition, their conductive values are too high to explain the conductivity-depth profiles in the transition zone obtained by the semi-global electromagnetic induction studies. However, the laboratory-based model by Yoshino et al. (2008a) showed three conductivity jumps at depths 410 km for wadsleyite–ringwoodite transition, 520 km for wadsleyite–ringwoodite transition and 660 km for post-spinel transition, and demonstrated that dry mantle model can explain the current geophysical observation beneath the Pacific Ocean by Kuvshinov et al. (2005). If we consider the results from Huang et al. (2005), who reported larger effects of water on electrical conductivity of wadsleyite and ringwoodite, the estimated water content is smaller than 0.1 wt.%.

5.4 High Conductivity Anomaly Near the Core-Mantle Boundary

Measured changes of a few milliseconds in Earth's length of day on decadal timescales have been considered by the exchange of angular momentum between the solid mantle and fluid core (Holme 1998), although EM coupling is not the only mechanism of transferring momentum between the core and mantle. If a layer with a high electrical conductivity

above the core-mantle boundary exists, it would enhance the electromagnetic coupling between the fluid core and solid mantle. The conductance of this layer requires $>10^8$ S to explain change of the length of a day. However, silicate perovskite does not have such a high electrical conductivity (Katsura et al. 1998; Xu et al. 1998b). Even if molten iron can penetrate from the outer core into the solid mantle, the depth of penetration of molten iron into the solid mantle would be not enough. Hence, the enhancement of the electrical conductivity of the solid mantle by penetration of molten iron would not be enough to explain the electromagnetic coupling between the core and the mantle. Post-perovskite ($CaIrO_3$-type crystal structure) could be present in the D" layer below about a 2,600-km depth (Murakmi et al. 2004). Ono et al. (2006) predicted a possibility that post-perovskite could enhance the conductivity at the lowermost mantle based on the high electrical conductivity of $CaIrO_3$-type Al_2O_3. Recently, Ohta et al. (2008) reported that $(Mg,Fe)SiO_3$ post-perovskite has much higher conductivity than silicate perovskite, and demonstrated that a presence of $\sim$300 km thickness post-perovskite layer can explain high conductance in the mantle estimated from change of the length of a day.

6 Concluding Remarks

Although data inconsistency among some laboratories still remains due to the difficulty of conductivity measurement under high-pressure condition, comprehensive collection of high-pressure conductivity data for mantle minerals yields some significant features of electrical conductivity of mantle minerals. Electrical conductivity of the main mantle constituent minerals increases in order of olivine, wadsleyite, ringwoodite, perovskite and post-perovskite. Under the Earth's mantle condition, hopping (small polaron) conduction can be considered as a dominant conduction mechanism in mantle minerals. Activation enthalpy for small polaron conduction becomes lower for minerals being stable under higher-pressure. If we consider only small polaron conduction, at least three conductivity jumps would be present at 410, 520 and 660 km discontinuities due to the phase transformation. Electrical conductivity increases with increasing water and iron contents. Activation energy for proton and hopping (small polaron) conduction decreases with increasing hydrogen and iron concentration, respectively. At high temperatures corresponding to the mantle condition, a contribution of proton conduction to the electrical conductivity of minerals becomes smaller due to the masking by small polaron conduction with higher activation energy. Therefore, a small difference of iron content may produce the large difference of conductivity.

Acknowledgments I wish to express my sincere thanks to the Program Committee and LOC of the Beijing workshop, who offered me a chance to prepare and deliver this review. I am grateful to T. Katsura, E. Ito, D. Yamazaki, K. Baba, T. Koyama, H. Toh and H. Utada for discussion. The comments of two anonymous reviewers aided in improving the manuscript.

References

Badro J et al (2003) Iron partitioning in Earth's mantle: toward a deep lower mantle discontinuity. Science 300:789–791

Bolfan-Cassanova N, Keppler H, Rubie DC (2000) Water partitioning between nominally anhydrous minerals in the $MgO–SiO_2–H_2O$ system up to 24 GPa: implications for the distribution of water in the Earth's mantle. Earth Planet Sci Lett 182:209–221

Brodholt JP (2000) Pressure-induced changes in the compression mechanism of aluminous perovskite in the earth's mantle. Nature 407:620–622
Bullen KE (1937) Note on the density and pressure inside the Earth. J R Soc NZ 67:122–124
Constable S (2006) SEO3: a new model of olivine electrical conductivity. Geophys J Int 166:435–437
Constable S, Constable C (2004) Observing geomagnetic induction in magnetic satellite measurements and associated implications for mantle conductivity. Geochem Geophys Geosys 5:Q01006
Constable SC, Shankland TJ, Duba AG (1992) The electrical conductivity of an isotropic olivine mantle. J Geophys Res 97:3397–3404
Debye PP, Conwell EM (1954) Electrical properties of *N*-type germanium. Phys Rev 93:693–706
Dobson DP (2003) Oxygen ionic conduction in $MgSiO_3$ perovskite. Phys Earth Planet Inter 139:55–64
Dobson DP, Brodholt JP (2000) The electrical conductivity of the lower mantle phase magnesiowüstite at high temperatures and pressures. J Geophys Res 105:531–538
Dobson DP, Richmond NC, Brodholt JP (1997) A high temperature electrical conduction mechanism in the lower mantle phase $(Mg, Fe)_{1-X}O$. Science 275:1779–1781
Du Frane WL, Roberts JJ, Toffelmier DA, Tyburczy JA (2005) Anisotropy of electrical conductivity in dry olivine. Geophys Res Lett 32:L24315
Duba AG, von der Gönna (1994) Comment on change of electrical conductivity of olivine associated with the olivine-spinel transition. Phys Earth Planet Int 82:75–77
Evans RL, Hirth G, Baba K, Forsyth D, Chave A, Mackie R (2005) Geophysical evidence from the MELT area for compositional controls on oceanic plates. Nature 437:249–252
Fei Y, Mao HK (1994) In situ determination of the NiAs phase of FeO at high pressure and high temperature. Science 266:1678–1680
Gaillard F, Malki M, Iacono-Marziano G, Pichavant M, Scaillet B (2008) Carbonatite melts and electrical conductivity in the asthenosphere. Science 322:1363–1365
Glover PWJ, Vine FJ (1992) Electrical conductivity of carbon bearing granulite at raised temperatures and pressures. Nature: 360:723–726
Glover PWJ, Ross RG, Jolly H (1990) The measurement of saturated rock electrical conductivity at lower crustal temperatures and high pressures. High Press Res 5:705–707
Goddat A, Peyronneau J, Poirier JP (1999) Dependence on pressure of conduction by hopping of small polarons in minerals mantle. Phys Chem Mineral 27:81–87
Hiraga T, Anderson IM, Kohlstedt DL (2004) Grain boundaries as a reservoir of incompatible elements in the Earth's mantle. Nature 427:699–704
Hirose K, Fei Y, Ma Y, Mao H–K (1999) The fate of subducted basaltic crust in the Earth's lower mantle. Nature 397:53–56
Hirsch LM, Shankland TJ (1993) Quantitative olivine-defect chemical model: insights on electrical conduction, diffusion, and the role of Fe content. Geophys J Int 114:21–35
Hirsch LM, Shankland TJ, Duba AG (1993) Electrical conduction and polaron mobility in Fe-bearing olivine. Geophys J Int 114:36–44
Holme R (1998) Electromagnetic core–mantle coupling, I, explaining decadal changes in the length of day. Geophys J Int 132:167–180
Huang X, Xu Y, Karato S (2005) Water content in the transition zone from electrical conductivity of wadsleyite and ringwoodite. Nature 434:746–749
Irifune T, Ringwood AE (1993) Phase transformations in subducted oceanic crust and buoyancy relationships at depths of 600–800 km in the mantle. Earth Planet Sci Lett 117:101–110
Irifune T, Sekine T, Ringwood AE, Hibberson WO (1986) The eclogite-garnetite transformation at high pressure and some geophysical implications. Earth Planet Sci Lett 77:245–256
Ito E, Takahashi E (1989) Post-spinel transformations in the system Mg_2SiO_4–Fe_2SiO_4 and some geophysical implications. J Geophys Res 94:10637–10646
Karato S (1990) The role of hydrogen in the electrical conductivity of the upper mantle. Nature 347:272–273
Karato S, Dai L (2009) Comments on "Electrical conductivity of wadsleyite as a function of temperature and water content" by Manthilake et al. Phys Earth Planet Int 174:19–21
Katsura T, Ito E (1996) Determination of Fe–Mg partitioning between perovskite and magnesiowüstite. Geophys Res Lett 23:2005–2008
Katsura T, Sato K, Ito E (1998) Electrical conductivity of silicate perovskite at lower-mantle conditions. Nature 395:493–495
Katsura T, Yokoshi S, Kawabe K, Shatskiy A, Okube M, Fukui H, Ito E, Nozawa A, Funakoshi K (2007) Pressure dependence of electrical conductivity of (Mg, Fe)SiO3 ilmenite. Phys Chem Mineral 34: 249–255
Kawai N (1966) A static high pressure apparatus with tapered multi-piston formed a sphere I. Proc Jpn Acad 42:285–288

Kawai N, Endo S (1970) The generation of ultrahigh hydrostatic pressure by a split sphere apparatus. Rev Sci Instrum 41:425–428
Keppler H, Kantor I, Dubrovinsky LS (2007) Optical absorption spectra of ferropericlase to 84 GPa. Am Mineral 92:433–436
Kittel C (1996) Introduction to solid state physics, 7th edn. Wiley, New York 673 pp
Kohlstedt DL, Mackwell SJ (1998) Diffusion of hydrogen and intrinsic point defects in olivine. Z Phys Chem 207:147–162
Kohlstedt DL, Keppler H, Rubie DC (1996) Solubility of water in the α, β and γ phases of $(Mg, Fe)_2SiO_4$. Contrib Mineral Petrol 123:345–357
Kondo T, Sawamoto H, Yoneda A, Kato T, Matsumoto A, Yagi T (1989) Ultrahigh-pressure and high temperature generation by use of the MA8 system with sintered diamond anvils. High Temp High Press 25:105–112
Kuvshinov A, Olsen N (2006) A global model of mantle conductivity derived from 5 years of CHAMP, Ørsted, and SAC-C magnetic data. Geophys Res Lett 33:L18301
Kuvshinov A, Utada H, Avdeev D, Koyama T (2005) 3-D modelling and analysis of *Dst C*-responses in the North Pacific Ocean region, revisited. Geophys J Int 160:505–526
Lauterbach S, McCammon CA, van Aken P, Langenhorst F, Seifert F (2000) Mössbauer and ELNES spectroscopy of (Mg, Fe)(Si, Al)O_3 perovskite: a highly oxidised component of the lower mantle. Contrib Mineral Petrol 138:17–26
Lay T, Helmberger DV (1983) A lower mantle *S*-wave triplication and the shear velocity structure of D". Geophys J R Astron Soc 75:799–838
Lay T, Williams Q, Garnero EJ (1998) The core-mantle boundary layer and deep mantle dynamics. Nature 392:461–468
Li X, Jeanloz R (1990a) Laboratory studies of the electrical conductivity of silicate perovskite at high pressures and temperatures. J Geophys Res 95:5067–5078
Li X, Jeanloz R (1990b) High pressure–temperature electrical conductivity of magnesiowüstite as a function of iron oxide concentration. J Geophys Res 95:21609–21612
Lin J-F et al (2005) Spin transition of iron in magnesiowüstite in Earth's lower mantle. Nature 436:377–380
Lin J-F, Weir ST, Jackson DD, Evans WJ, Vohra YK, Qiu W, Yoo C-S (2007a) Electrical conductivity of the lower-mantle ferropericlase across the electronic spin transition. Geophys Res Lett 34:L16305. doi: 10.1029/2007GL030523
Lin J-F, Vanko G, Jacobsen SD, Iota V, Strurzhkin VV, Prakapenka VB, Kuznetsov A, Yoo C-S (2007b) Spin transition zone in Earth's lower mantle. Science 317:1740–1743
Lizarralde D, Chave AD, Hirth G, Schultz A (1995) A Northern Pacific mantle conductivity profile from long-period magnetotelluric sounding using Hawaii to California submarine cable data. J Geophys Res 100:17837–17854
Mackwell SJ, Kohlstedt DL (1990) Diffusion of hydrogen in olivine: implications for water in mantle. J Geophys Res 95:5079–5088
Manthilake G, Matsuzaki T, Yoshino T, Yamashita S, Ito E, Katsura T (2009) Electrical conductivity of wadsleyite as a function of temperature and water content. Phys Earth Planet Int 174:10–18
Mao HK (1973) Observation of optical absorption and electrical conductivity in magnesiowüstite at high pressures. Year B Carnegie Inst Wash 72:554–557
Mao HK, Shen G, Hemley RJ, Duffy TS (1998) X-ray diffraction with a double hot-plate laser-heated daiamond anvil cell. In: Manghnani MH, Yagi T (eds) Properties of earth and planetary materials at high pressure and temperature. Am Geophys Union, Washington, pp 27–34
McCammon C (1997) Perovskite as a possible sink for ferric iron in the lower mantle. Nature 387:694–696
McCammon C (2005) The paradox of mantle redox. Science 308:807–808
Ming LC, Bassett WA (1974) Laser heating in the diamond anvil press up to 2000°C sustained and 3000°C pulsed at pressures up to 260 kilobars. Rev Sci Instrum 45:1115–1118
Murakmi M, Hirose K, Kawamura K, Sata N, Ohishi Y (2004) Post-perovskite phase transition in $MgSiO_3$. Science 304:855–858
Neal SL, Mackie RL, Larsen JC et al (2000) Variations in the electrical conductivity of the upper mantle beneath North America and the Pacific Ocean. J Geophys Res 105:2829–2842
Ohta K, Hirose K, Onoda S, Shimizu K (2007) The effect of iron spin transition on electrical conductivity of magnesiowüstite. Proc Jpn Acad, Ser B 83:97–100
Ohta K, Onoda S, Hirose K, Shinmyo R, Shimizu K, Sata K, Ohishi Y, Yasuhara A (2008) The electrical conductivity of post-perovskite in Earth's D" layer. Science 320:89–91
Ohtani E, Kagawa K, Shimomura O (1989) High-pressure generation by a multiple anvil system with sintered diamond anvils. Rev Sci Instrum 60:922–925

Olsen N (1998) The electrical conductivity of the mantle beneath Europe derived from C-responses from 3 to 720 hr. Geophys. J. Int. 133:298–308
Olsen N (1999) Induction studies with satellite data. Surv Geophys 20:309–340
Omura K (1991) Change of electrical conductivity of olivine associated with the olivine-spinel transition. Phys Earth Planet Int 65:292–307
Omura K, Kurita K, Kumazawa M (1989) Experimental study of pressure dependence of electrical conductivity of olivine at high temperatures. Phys Earth Planet Int 57:291–303
Ono S, Ito E, Katsura T (2001) Mineralogy of subducted basaltic crust (MORB) from 25 to 37 GPa, and chemical heterogeneity of the lower mantle. Earth Planet Sci Lett 190:57–63
Ono S, Oganov AR, Koyama T, Shimizu H (2006) Stability and compressibility of the high pressure phases of Al_2O_3 up to 200 GPa: implications for the electrical conductivity of the base of the lower mantle. Earth Planet Sci Lett 246:326–335
Persson K, Bengtson A, Ceder G, Morgan D (2006) Ab initio study of the composition dependence of the pressure-induced spin transition in the $(Mg_{1-x}, Fe_x)O$ system. Geophys Res Lett 33:L16306. doi:10.1029/2006GL026621
Peyronneau J, Poirier JP (1989) Electrical conductivity of the Earth's lower mantle. Nature 342:537–539
Roberts JJ, Tyburczy JA (1991) Frequency dependent electrical properties of polycrystalline olivine compacts. J Geophys Res 96:16205–16222
Roberts JJ, Tyburczy JA (1993) Impedance spectroscopy of single and polyscrystalline olivine: evidence for grain boundary transport. Phys Chem Minerals 20:19–26
Roberts JJ, Tyburczy JA (1999) Partial melt electrical conductivity: influence of melt compositon. J Geophys Res 104:737–747
Romano C, Poe BT, Kreidie N, McCammon CA (2006) Electrical conductivities of pyrope-almandine garnets up to 19 GPa and 1700°C. Am Mineral 91:1371–1377
Schock RN, Duba AG, Shankland TJ (1989) Electrical conduction in olivine. J Geophys Res 94:5829–5839
Seifert KF, Will G, Voigt R (1982) Electrical conductivity measurements on synthetic pyroxenes $MgSiO_3$–$FeSiO_3$ at high pressures and temperatures under defined thermodynamic conditions. In: Schreyer W (ed) High-pressure researches in geoscience. Schweizerbart'sche, Stuttgart, pp 419–432
Sempolinski DR, Kingery WD, Tuller HL (1980) Electrical conductivity of single crystalline magnesium oxide. J Am Ceram Soc 63:669–675
Shankland TJ, Duba AG (1990) Standard electrical conductivity of isotropic, homogeneous olivine in the temperature range 1200–1500°C. Geophys J Int 103:25–31
Shankland TJ, Peyronneau J, Poirier J-P (1993) Electrical conductivity of the earth's lower mantle. Nature 366:453–455
Sturhahn W, Jackson JM, Lin J-F (2005) The spin state of iron in minerals of Earth's lower mantle. Geophys Res Lett 32:L12307. doi:10.1029/2005GL022802
Sung C-M, Sung M (1996) Carbon nitrite and other speculative super hard materials. Material Chem Phys 43:1–18
Takahashi E, Ito E (1987) Mineralogy of mantle periodotite along a model geotherm up to 700 km depth. In: Manghnani MH, Shono Y (eds) High-pressure research in mineral physics. American Geophysical Union, Washington, pp 427–437
Tarits P, Hautot S, Perrier F (2004) Water in the mantle: results from electrical conductivity beneath the French Alps. Geophys Res Lett 31:L06612. doi:10.1029/2003GL019277
Ten Grotenhuis SM, Drury MR, Spiers CJ, Peach CJ (2005) Melt distribution in olivine rocks beased on electrical conductivity measurements. J Geophys Res 110:B12201
Tsuchiya T, Wentzcovitch RM, da Silva CRS, de Gironcoli S (2006) Spin transition in magnesiowüstite in Earth's lower mantle. Phys Rev Lett 96:198501. doi:10.1103/PhysRevLett.96.198501
Utada H, Koyama T, Shimizu H et al (2003) A semi-global reference model for electrical conductivity in the mid-mantle beneath the north Pacific region. Geophys Res Lett 31:1194. doi:10.1029/2002GL016902
Wanamaker BJ, Duba AG (1993) Electrical conductivity of San Carlos olivine along [100] under oxygen- and pyroxene-buffered conditions and implications for defect equilibria. J Geophys Res 98:489–500
Wang D, Mookherjee M, Xu Y et al (2006) The effect of water on electrical conductivity of olivine. Nature 443:977–980
Wood BJ, Nell J (1991) High-temperature electrical conductivity of the lower-mantle phase (Mg, Fe)O. Nature 351:309–311
Wood BJ, Rubie DC (1996) The effect of alumina on phase transformations at the 660 km discontinuity from Fe–Mg partitioning experiments. Science 273:1522–1524
Xu Y, McCammon C (2002) Evidence for ionic conductivity in lower mantle (Mg, Fe)(Si, Al)O_3 perovskite. J Geophys Res 107:2251. doi:10.1029/2001JB000677

Xu Y, Shankland TJ (1999) Electrical conductivity of orthopyroxene and its high pressure phases. Geophys Res Lett 22:2645–2648

Xu Y, Poe BT, Shankland TJ et al (1998a) Electrical conductivity of olivine, wadsleyite and ringwoodite under upper-mantle condition. Science 280:1415–1418

Xu Y, McCammon C, Poe BT (1998b) Effect of alumina on the electrical conductivity of silicate perovskite. Science 282:922–924

Xu Y, Shankland TJ, Duba AG (2000a) Pressure effect on electrical conductivity of olivine. Phys Earth Planet Int 118:149–161

Xu Y, Shankland TJ, Poe BT (2000b) Laboratory-based electrical conductivity in the Earth's mantle. J Geophys Res 105:27865–27875

Yoshino T, Katsura T (2009) Effect of iron content on electrical conductivity of ringwoodite, with implications for electrical structure in the mantle transition zone. Phys Earth Planet Int 174:3–9

Yoshino T, Walter MJ, Katsura T (2003) Core formation in planetesimals triggered by permeable flow. Nature 422:154–157

Yoshino T, Walter MJ, Katsura T (2004) Connectivity of molten Fe alloy in peridotite based on in situ electrical conductivity measurements: implications for core formation in terrestrial planets. Earth Planet Sci Lett 222:625–643

Yoshino T, Matsuzaki T, Yamashita S, Katsura T (2006) Hydrous olivine unable to account for conductivity anomaly at the top of the asthenosphere. Nature 443:973–976

Yoshino T, Manthilake G, Matsuzaki T, Katsura T (2008a) Dry mantle transition zone inferred from electrical conductivity of wadsleyite and ringwoodite. Nature 451:326–329

Yoshino T, Nishi M, Matsuzaki T, Yamazaki D, Katsura T (2008b) Electrical conductivity of majorite garnet and its implications for electrical structure in the mantle transition zone. Phys Earth Planet Int 170:193–200

Yoshino T, Yamazaki D, Ito E, Katsura T (2008c) No interconnection of ferro-periclase in post-spinel phase inferred from conductivity measurement. Geophys Res Lett 35:L22303. doi:10.1029/2008GL035932

Yoshino T, Matsuzaki T, Shatzkiy A, Katsura T (2009) The effect of water on the electrical conductivity of olivine aggregates and its implications for the electrical structure of the upper mantle. Earth Planet Sci Lett. doi:10.1016/j.epsl.2009.09.032